

GRVFL-MV: Graph Random Vector Functional Link Based on Multi-View Learning

M. Tanveer^{a,*}, R. K. Sharma^a, M. Sajid^a, A. Quadir^a

^a*Department of Mathematics, Indian Institute of Technology Indore, Simrol, Indore, 453552, Madhya Pradesh, India*

Abstract

The classification performance of the random vector functional link (RVFL), a randomized neural network, has been widely acknowledged. However, due to its shallow learning nature, RVFL often fails to consider all the relevant information available in a dataset. Additionally, it overlooks the geometrical properties of the dataset. To address these limitations, a novel graph random vector functional link based on multi-view learning (GRVFL-MV) model is proposed. The proposed model is trained on multiple views, incorporating the concept of multiview learning (MVL), and it also incorporates the geometrical properties of all the views using the graph embedding (GE) framework. The fusion of RVFL networks, MVL, and GE framework enables our proposed model to achieve the following: i) *efficient learning*: by leveraging the topology of RVFL, our proposed model can efficiently capture nonlinear relationships within the multi-view data, facilitating efficient and accurate predictions; ii) *comprehensive representation*: fusing information from diverse perspectives enhance the proposed model's ability to capture complex patterns and relationships within the data, thereby improving the model's overall generalization performance; and iii) *structural awareness*: by employing the GE framework, our proposed model leverages the original data distribution of the dataset by naturally exploiting both intrinsic and penalty

*Corresponding author

Email addresses: mtanveer@iiti.ac.in (M. Tanveer), msc2203141001@iiti.ac.in (R. K. Sharma), phd2101241003@iiti.ac.in (M. Sajid), mscphd2207141002@iiti.ac.in (A. Quadir)

subspace learning criteria. The evaluation of the proposed GRVFL-MV model on various datasets, including 27 UCI and KEEL datasets, 50 datasets from Corel5k, and 45 datasets from AwA, demonstrates its superior performance compared to baseline models. These results highlight the enhanced generalization capabilities of the proposed GRVFL-MV model across a diverse range of datasets.

Keywords: Artificial neural network, randomized neural network, random vector functional link neural network (RVFL), multiview learning, graph embedding framework.

1. Introduction

The artificial neural networks (ANNs) belong to the class of non-parametric learning methods that are used for estimating or approximating functions that may depend on a large number of inputs and outputs [54]. Inspired by the topology of biological neural networks, ANNs have found applications in diverse domains, such as image recognition [37], Alzheimer’s disease diagnosis [44, 45], stock price prediction [13], brain age prediction [43], and so on. The efficacy of ANNs depends upon several factors, including the quality and quantity of data, computational resources, and the effectiveness of underlying algorithms [1]. The ANNs are trained by optimizing a cost function, which quantifies the disparity between model predictions and actual observations. The adjustment of the network’s weights and biases is facilitated through back-propagation, employing an iterative technique known as the gradient descent (GD) method. To enhance the agreement between predicted outcomes and actual observations, the optimization process requires fine-tuning the network’s weights and biases. Nevertheless, GD-based algorithms come with inherent limitations, including slow convergence [20], difficulty in achieving global minima [12] and heightened sensitivity to the selection of learning rate and the point of initialization [34].

Randomized neural networks (RNNs) [36] have emerged as a unique solution to overcome the difficulties faced in training ANNs using gradient descent (GD) methods. Un-

like conventional ANNs, RNNs adopt a distinct approach where the network’s weights and biases are randomly selected from a specified range and remain constant throughout the training process. The determination of output layer parameters in RNNs is achieved through a closed-form solution [38], as opposed to iterative-based optimization techniques commonly employed in traditional ANNs. The prominent examples of RNNs include the random vector functional link (RVFL) network [29, 26] and the extreme learning machines (ELM) [16]. RVFL has garnered significant attention within the realm of RNNs due to its distinctive features, including direct connections between input and output layers that improve generalization performance, a straightforward architecture aligned with Occam’s Razor principle and PAC learning theory [22], a reduced number of parameters, and the universal approximation capability [18]. Furthermore, the direct connections help to regulate the randomness in RVFL [54, 35], while the output parameters are computed analytically through methods like pseudo-inverse or least-square techniques.

Various enhancements have been implemented to optimize the learning capabilities of RVFL, with notable advancements such as the sparse pre-trained random vector functional link (SP-RVFL) network [57] and the discriminative manifold RVFL neural network (DM-RVFLNN) [24]. The SP-RVFL network utilizes diverse weight initialization methods to improve the generalization performance of standard RVFL models, while the DM-RVFLNN integrates manifold learning with a soft label matrix to enhance the model’s discriminative capacity by increasing the margin between samples from different classes. In addition, techniques such as manifold learning based on an in-class similarity graph have been employed to enhance the compactness and similarity of samples within the same class. To address noise and outliers, Cui et al. [5] proposed an RVFL-based approach that incorporates a novel feature selection (FS) technique, enhancing the efficiency and robustness of RVFL through the augmented Lagrangian method. Furthermore, the integration of a kernel function into RVFL has led to the development of the kernel exponentially extended RVFL

network (KERVFLN) [3], demonstrating the adaptability and potential of RVFL in various machine learning applications. Recent advancements in RVFL theory include RVFL+, kernel RVFL+ (KRVFL+) [55], incremental learning paradigm with privileged information for RVFL (IRVFL+), and improved fuzziness-based RVFL [6, 2], showcasing the ongoing evolution and versatility of RVFL models in addressing diverse machine-learning challenges, including multilabel classification tasks using RNNs. Some recent advancements in RVFL theory include neuro-fuzzy RVFL for classification and regression problems [35], kernel ridge regression-based randomized network for brain age classification and estimation [30], domain-incremental learning without forgetting based on RVFL [25], etc.

In various real-world applications, a multitude of characteristics is often observed, requiring representation through multiple feature sets. This leads to the prevalence of multiview data, where information from various measurement methods is collected to comprehensively capture the nuances of each example rather than relying solely on a single feature set. For instance, a picture can be described by color or texture features, and a person can be identified by face or fingerprints [48]. Web pages serve as a quintessential example of multimodal data, where one feature vector encapsulates the words within the webpage text, while another feature vector captures the words present in the links pointing to the webpage from other pages. While individual views may suffice for specific learning tasks, there is potential for enhancement by fusing insights from multiple data representations [14]. Multiview learning (MVL), a well-established collection of techniques, holds significant potential as multi-modal datasets become increasingly accessible [50]. MVL models are often developed under the supervision of the consensus or complimentary principles [31, 33] to ensure the effectiveness of an algorithm. The consensus principle aims to enhance the performance of classifiers for each view by maximizing consistency across multiple viewpoints. Conversely, the complementarity principle emphasizes the importance of providing complementary data from diverse perspectives to offer a comprehensive and

accurate description of the object.

The fusion of the graph embedding (GE) [51] framework with the RVFL model has played a crucial role in enhancing the learning process of RVFL. By incorporating the GE framework, the RVFL model is able to capture the geometric relationships present within the dataset, which were previously overlooked [26]. To incorporate the geometrical relationships within a dataset, Malik et al. [28] introduced the graph-embedded intuitionistic fuzzy weighted RVFL (GE-IFWRVFL) model. This model not only integrates the intuitionistic fuzzy (IF) membership scheme to handle noisy data and outliers but also preserves the geometric characteristics through the GE framework. The fusion of IF and GE with RVFL has proven to enhance the resilience and performance of the RVFL significantly. Recent advancements in RVFL have seen the utilization of GE framework in extended graph-embedded RVFL (EGERVFL) and graph-embedded intuitionistic fuzzy RVFL network for class imbalance learning (GE-IFRVFL-CIL) as proposed in [27] and [11] respectively. The experimental results from [28, 27, 11], along with studies in [26], strongly support the notion that the performance of RVFL is greatly improved through the fusion of the GE framework. This emphasizes the importance of considering the geometric attributes of a dataset in the learning process to enhance the overall performance of RVFL.

RVFL is categorized as a shallow learning algorithm due to its single hidden layer, which may potentially hinder its ability to fully grasp complex patterns and subtle nuances in a dataset. While RVFL may excel in specific classification tasks, its architecture could limit its capability to accurately interpret intricate patterns or extract detailed features from the dataset. The simplicity of RVFL’s architecture offers advantages in terms of computational efficiency and ease of implementation. However, when confronted with datasets containing intricate patterns or nuanced relationships among variables, more sophisticated learning frameworks are necessary to effectively capture the underlying complexities inherent in

the dataset. To mitigate the limitations imposed by the subsurface learning nature of RVFL, presenting the same information from multiple perspectives can offer a solution. By training RVFL on multiple views of the data, it becomes possible to compensate for its inherent learning structure and enhance its ability to comprehend intricate patterns and subtle nuances within the dataset. Hence, leveraging the multiview learning (MVL) framework can significantly enhance the learning efficiency of RVFL.

Recognizing the importance of a dataset’s inherent geometrical characteristics and MVL, we propose the novel graph random vector functional link based on multi-view learning (GRVFL-MV). The GRVFL-MV method incorporates the intrinsic and penalty graphical representations of multiview datasets within the GE framework, thereby capturing the geometrical properties of the multiview data. By fusing the MVL and GE framework with RVFL, the learning capabilities of RVFL are greatly enhanced, allowing it to effectively tackle classification challenges. In order to ensure simplicity and effectiveness, the proposed GRVFL-MV model incorporates two views at a time. This strategy allows for a balance between complexity and performance, as it utilizes the complementary information from these two views to enhance effectiveness while still maintaining simplicity. By leveraging information from multiple views, GRVFL-MV significantly improves the classification performance of RVFL by integrating both geometric and discriminative information from both views using intrinsic and penalty-based subspace learning criteria within the GE framework.

The main contributions of this research are highlighted below:

- We present a generic framework that fuses random vector functional link (RVFL) with multiview learning (MVL) and graph embedding (GE) framework. This novel model is called the graph random vector functional neural network based on multi-view learning (GRVFL-MV).

- The proposed GRVFL-MV model is developed upon the foundation of the RVFL architecture, which is known for its simplicity and efficiency. However, it goes beyond the limitations of shallow learning of RVFL by integrating the concept of multiview learning (MVL). By leveraging multiple views, the model aims to enhance classification performance using multiple perspectives of the dataset.
- The proposed GRVFL-MV model integrates geometrical information from multiview data by embedding intrinsic and penalty subspace learning (SL) criteria within the GE framework. It employs local Fisher discriminant analysis (LFDA) [39] and graph regularization parameters to effectively utilize the GE framework.
- To trade off the information from multiple views, our proposed mathematical formulation includes a coupling term. This coupling term helps to mitigate errors between the views, resulting in improved generalization performance.
- Our experiments encompassed 27 UCI and KEEL datasets, 50 datasets from Corel5k, and 45 datasets from AWA. Through comprehensive statistical analyses, we demonstrate the superior generalization performance of our proposed model when compared to baseline models.

The paper is organized as follows: Section 2 provides a comprehensive overview of preliminary works. The mathematical derivation and the computational complexity of the proposed model are presented in Section 3. Section 4 presents the experimental results and statistical analyses. Finally, Section 5 concludes the paper and provides recommendations for future research.

2. Preliminary Works

In this section, we start with fixing some notations and then provide a detailed description of random vector functional (RVFL) [29]. We also give the literature overview of

multiview learning (MVL) and review the graph embedding [49] framework.

2.1. Notations

For simplicity, we consider the notations w.r.t. two-views. Let the two-view training dataset $S = \{(x_i^A, x_i^B, y_i) | x_i^A \in \mathbb{R}^{1 \times n}, x_i^B \in \mathbb{R}^{1 \times m}, y_i \in \{-1, 1\}, i = 1, 2, \dots, l\}$, where x_i^A and x_i^B represents the feature vector of each data sample corresponding to *view - A* and *view - B*, respectively and y_i represents the label of the individual data for both the views. Let $X_A \in \mathbb{R}^{l \times n}$ and $X_B \in \mathbb{R}^{l \times m}$ be the input matrices for *view - A* and *view - B*, respectively and $Y_{true} \in \mathbb{R}^{l \times 2}$ represents the one hot encoding matrix of the output. $(\cdot)^t$ represents the transpose operator.

2.2. Random Vector Functional Link Neural Network (RVFL)

The RVFL [29] model consists of an input layer, a hidden layer, and an output layer. The input and output layers are connected through the hidden layer, which acts as a bridge between them. Notably, the original features are also directly passed to the output layer because of the direct connections between the input and output layers. During the training process, the weights connecting the input and hidden layers, as well as the biases at the hidden layer, are randomly generated. Once generated, these parameters remain fixed and do not require any adjustments during the training phase. In terms of determining the output weight matrix connecting the input layer and the hidden layer to the output layer, the least squares or pseudo-inverse methods are employed, providing an analytical solution.

Consider a training matrix X with dimensions $l \times p$. Let W_1 be a weight matrix with dimensions $p \times h$, where the values are randomly generated from a uniform distribution within the range of $[-1, 1]$ and $B_1 \in \mathbb{R}^{l \times h}$ (all the columns are identical) be the randomly generated bias matrix. To obtain the hidden layer matrix, also called the randomized feature layer, denoted as H_1 , we apply a nonlinear activation function ϕ to the matrix

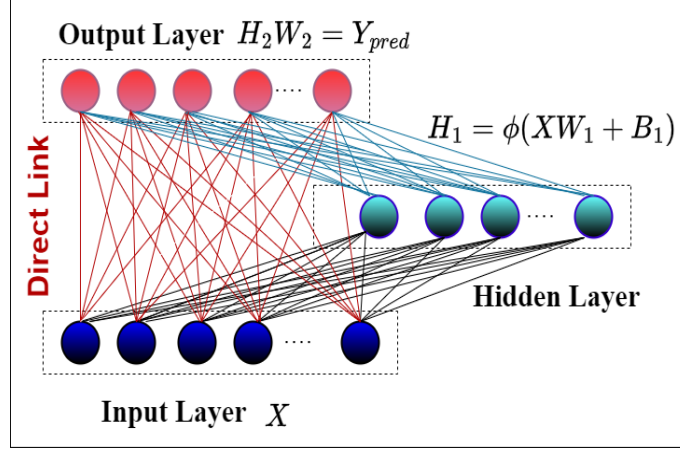


Figure 1: The architecture of RVFL model.

$XW_1 + B_1$. Consequently, the hidden layer matrix H_1 can be expressed as:

$$H_1 = \phi(XW_1 + B_1). \quad (1)$$

Therefore, the matrix H_1 can be represented as:

$$H_1 = \begin{bmatrix} \phi(x_1w_1 + b_1) & \cdots & \phi(x_1w_h + b_h) \\ \vdots & \vdots & \vdots \\ \phi(x_pw_1 + b_1) & \cdots & \phi(x_pw_h + b_h) \end{bmatrix},$$

where $x_i \in \mathbb{R}^{1 \times p}$ and $w_j \in \mathbb{R}^{p \times 1}$ represent the i^{th} row of X and the j^{th} column of W_1 , respectively. The term b_j represents the bias of the j^{th} hidden node.

Let H_2 be a concatenated matrix of features from the input and hidden layers, represented as $H_2 = \begin{bmatrix} X & H_1 \end{bmatrix} \in \mathbb{R}^{l \times (p+h)}$. Here, X represents the input features, and H_1 represents the output of the hidden layer. Let W_2 denote the weights matrix connecting the concatenation of input (X) and hidden (H_1) layers to the output layer, with dimensions $W_2 \in \mathbb{R}^{(p+h) \times 2}$. The predicted output matrix $Y_{pred} \in \mathbb{R}^{l \times 2}$ of the RVFL is calculated using

the following matrix equation:

$$H_2 W_2 = Y_{pred}. \quad (2)$$

The optimization problem of (2) is given as:

$$\begin{aligned} \min_{W_2} \quad & \frac{1}{2} \|W_2\|_2^2 + \frac{c}{2} \|\xi\|_2^2 \\ \text{s.t.} \quad & H_2 W_2 - Y_{true} = \xi, \end{aligned} \quad (3)$$

where c is a regularization parameter.

The solution of (3) is given by:

$$(W_2)_{min} = \begin{cases} (H_2^t H_2 + \frac{1}{c} I)^{-1} H_2^t Y_{true}, & (p+h) \leq l \\ H_2^t (H_2 H_2^t + \frac{1}{c} I)^{-1} Y_{true}, & l < (p+h) \end{cases} \quad (4)$$

2.3. Graph Embedding (GE)

The concept of graph embedding (GE) framework [49] aims to capture the underlying graphical structure of data in a vector space. In this framework, a given input matrix X is utilized to define the intrinsic graph $\mathcal{G}^{int} = \{X, \Delta^{int}\}$ and the penalty graph $\mathcal{G}^{pen} = \{X, \Delta^{pen}\}$ for the purpose of subspace learning (SL) [51]. The similarity weight matrix $\Delta^{int} \in \mathbb{R}^{l \times l}$ incorporates weights that represent the pairwise relationships between the vertices in X . Conversely, the penalty weight matrix $\Delta^{pen} \in \mathbb{R}^{l \times l}$ assigns penalties to specific relationships among the graph vertices. The optimization problem for graph embedding is formulated as follows:

$$\begin{aligned} v^* &= \underset{tr(v_0^t X^t \cup X v_0) = d}{\operatorname{argmin}} \sum_{k \neq l} \|v_0^t x_k - v_0^t x_l\| \Delta_{kl}^{int} \\ &= \underset{tr(v_0^t X^t \cup X v_0) = d}{\operatorname{argmin}} \operatorname{tr}(v_0^t X^t \mathbb{L} X v_0) \end{aligned} \quad (5)$$

where $tr(\cdot)$ is the trace operator and d is a constant value. $\mathbb{L} = \mathbb{D} - \Delta^{int} \in \mathbb{R}^{l \times l}$ is a representation of the Laplacian matrix of the intrinsic graph \mathcal{G}^{int} , with the diagonal elements of \mathbb{D} being defined as $\mathbb{D}_{kk} = \sum_l \Delta_{kl}^{int}$. Moreover, $\mathbb{U} = \mathbb{L}^p = \mathbb{D}^p - \Delta^{pen}$ serves as the Laplacian matrix of the penalty graph \mathcal{G}^{pen} . The matrix v_0 is associated with the projection matrix. Equation (5) can be simplified to a generalized eigenvalue problem as shown in the form:

$$G_{int}s = \lambda G_{pen}s, \quad (6)$$

where $G_{int} = X^t \mathbb{L} X$ and $G_{pen} = X^t \mathbb{U} X$. This simplification implies that the transformation matrix will be constructed from the eigenvectors of the matrix $G = G_{pen}^{-1} G_{int}$, where G integrates the intrinsic and penalty graph connections of the data samples.

2.4. Literature Review on Multiview Learning (MVL)

Multiview learning (MVL) is an emerging area of research that holds significant promise in enhancing the generalization performance across various learning tasks. By integrating multiple feature sets, each offering unique and complementary insights, MVL has the potential to significantly improve overall model performance [59, 41, 42]. The abundance of diverse data types in practical applications has led to the development of MVL. In real-world scenarios, samples from different perspectives may reside in distinct spaces or exhibit vastly different distributions, often due to significant disparities between views [21, 23]. However, conventional approaches typically address such data by employing a cascade strategy, wherein multiview data is amalgamated into a single-view format through the concatenation of heterogeneous feature spaces into a homogeneous one. However, this cascading approach overlooks the distinctive statistical properties of each view and is plagued by the curse of dimensionality problems. One notable advantage of MVL is that it can enhance the performance of a standard single-view approach by leveraging manually generated multiple views.

In MVL, a distinct function is developed for each view, with the overall goal of constructing a unified function to optimize all individual functions jointly. This approach enhances the generalization performance of the framework across multiple views. According to Zhao et al. [59], MVL models can be categorized into three main groups: co-training style algorithms, co-regularization style algorithms, and margin consistency style algorithms. Co-training style algorithms focus on enhancing mutual agreement among diverse views. Conversely, co-regularization style algorithms aim to minimize discrepancies during the learning process. MVL learning has been successfully implemented in various hyper-plane based classifiers, such as SVM-2K [10], multiview twin support vector machine [47] (MvTSVM), deep multi-view multiclass TSVM [46], MVL with robust double-sided TSVM [53], etc. A notable application of MVL has been found in predicting DNA-binding protein using RVFL [32]. Furthermore, MVL has demonstrated its effectiveness across various application scenarios, including enhancing image classification, annotation, and retrieval performance [4], predicting financial distress [40], forecasting multiple stages of Alzheimer’s Disease progression [56], and identifying product adoption intentions from social media data [58]. MVL is now widely used in many various domains [17, 52] and research endeavors.

3. The Proposed Graph Random Vector Functional Link Neural Network based on Multi-View Learning (GRVFL-MV)

In this section, we introduce a novel GRVFL-MV, which fuses the RVFL with MVL. Our proposed model is structured to leverage the strengths of RVFL while incorporating both intrinsic and penalty graphical representations of multiview data through the GE framework. To derive the network output weights, the optimization process integrates subspace learning (SL) criteria, incorporating both intrinsic and penalty-based SL methodologies within the GE framework. To preserve the geometric structure effectively, we incorporate local Fisher discriminant analysis (LFDA) [39] into the GE framework. Additionally, we

introduce a regularization parameter for GE to enhance the learning process further. To trade off the error between multiple views, we introduce a coupling term in the primal optimization problem of the proposed model. This term minimizes the combined error from both views, resulting in an improved generalization performance for our model. The proposed optimization problem of the GRVFL-MV model is presented below:

$$\begin{aligned} \min_{\beta_1, \beta_2} \quad & \frac{c_1}{2} \|\xi_1\|_2^2 + \frac{c_2}{2} \|\xi_2\|_2^2 + \frac{c_3}{2} \|\beta_1\|_2^2 + \frac{1}{2} \|\beta_2\|_2^2 + \frac{\theta_1}{2} \|G_1^{1/2} \beta_1\|_2^2 + \frac{\theta_2}{2} \|G_2^{1/2} \beta_2\|_2^2 + \rho \xi_1^t \xi_2 \\ \text{s.t.} \quad & Z_1 \beta_1 - Y_{true} = \xi_1 \text{ and } Z_2 \beta_2 - Y_{true} = \xi_2, \end{aligned} \quad (7)$$

$$\text{where } Z_1 = \begin{bmatrix} X_A & H_A \end{bmatrix} \text{ and } Z_2 = \begin{bmatrix} X_B & H_B \end{bmatrix}. \quad (8)$$

$H_A = \phi(X_A W_A + B_A)$ and $H_B = \phi(X_B W_B + B_B)$, where $\phi(\cdot)$ is a non-linear activation function. W_A and B_A are the randomly initialized weight and bias matrices for *view - A* and W_B and B_B for *view - B*, respectively.

Optimization problem (7) has the following components:

1. Connections between the concatenated matrix Z_1 and the output layer are established by the weight matrix β_1 , while the weight matrix β_2 establishes connections between the Z_2 and the output layer. Minimizing $\|\beta_1\|_2^2$ and $\|\beta_2\|_2^2$ incorporates the structural risk minimization (SRM) principle.
2. G_1 and G_2 represent the graph embedding matrices w.r.t. *view - A* and *view - B*, respectively, and minimizing $\|G_1^{1/2} \beta_1\|_2^2$ and $\|G_2^{1/2} \beta_2\|_2^2$ facilitates the preservation of graph structural relationships between data points.
3. ξ_1 and ξ_2 represent the empirical errors in *view - A* and *view - B*, respectively. Minimizing $\|\xi_1\|_2^2$ and $\|\xi_2\|_2^2$ leads to the reduction of empirical errors in both views.
4. The term $\xi_1^t \xi_2$ acts as a coupling term that fuses information from both views and promotes the simultaneous minimization of errors in both views.

5. The variables θ_1 and θ_2 are graph regularization parameters, while c_1 , c_2 , and c_3 represent the regularization parameters and ρ is the coupling parameter.

The lagrangian of (7) is:

$$L = \frac{c_1}{2} \|\xi_1\|^2 + \frac{c_2}{2} \|\xi_2\|^2 + \frac{c_3}{2} \|\beta_1\|^2 + \frac{1}{2} \|\beta_2\|^2 + \frac{\theta_1}{2} \|G_1^{1/2} \beta_1\|^2 + \frac{\theta_2}{2} \|G_2^{1/2} \beta_2\|^2 + \rho \xi_1^t \xi_2 - \alpha_1^t (Z_1 \beta_1 - Y_{true} - \xi_1) - \alpha_2^t (Z_2 \beta_2 - Y_{true} - \xi_2). \quad (9)$$

Partially differentiating w.r.t. $\xi_1, \xi_2, \beta_1, \beta_2, \alpha_1$, and α_2 we get

$$\frac{\partial L}{\partial \xi_1} = c_1 \xi_1 + \rho \xi_2 + \alpha_1 = 0, \quad (10)$$

$$\frac{\partial L}{\partial \xi_2} = c_2 \xi_2 + \rho \xi_1 + \alpha_2 = 0, \quad (11)$$

$$\frac{\partial L}{\partial \beta_1} = c_3 \beta_1 + \theta_1 G_1 \beta_1 - Z_1^t \alpha_1 = 0, \quad (12)$$

$$\frac{\partial L}{\partial \beta_2} = \beta_2 + \theta_2 G_2 \beta_2 - Z_2^t \alpha_2 = 0, \quad (13)$$

$$\frac{\partial L}{\partial \alpha_1} = Z_1 \beta_1 - Y_{true} - \xi_1 = 0, \quad (14)$$

$$\frac{\partial L}{\partial \alpha_2} = Z_2 \beta_2 - Y_{true} - \xi_2 = 0. \quad (15)$$

Substituting (10) and (11) in (12) and (13) respectively, we get

$$c_3 \beta_1 + \theta_1 G_1 \beta_1 + Z_1^t (c_1 \xi_1 + \rho \xi_2) = 0, \quad (16)$$

$$\beta_2 + \theta_2 G_2 \beta_2 + Z_2^t (c_2 \xi_2 + \rho \xi_1) = 0. \quad (17)$$

Substituting the value of (14) and (15) in (16) and (17), we get

$$c_3 \beta_1 + \theta_1 G_1 \beta_1 + Z_1^t (c_1 (Z_1 \beta_1 - Y_{true}) + \rho (Z_2 \beta_2 - Y_{true})) = 0, \quad (18)$$

$$\beta_2 + \theta_2 G_2 \beta_2 + Z_2^t (c_2 (Z_1 \beta_1 - Y_{true}) + \rho (Z_2 \beta_2 - Y_{true})) = 0. \quad (19)$$

On simplifying, we get

$$c_3\beta_1 + \theta_1 G_1 \beta_1 + c_1 Z_1^t Z_1 \beta_1 + \rho Z_1^t Z_2 \beta_2 = Z_1^t (c_1 + \rho) Y_{true}, \quad (20)$$

$$\beta_2 + \theta_2 G_2 \beta_2 + c_2 Z_2^t Z_2 \beta_2 + \rho Z_2^t Z_1 \beta_1 = Z_2^t (c_2 + \rho) Y_{true}. \quad (21)$$

Finally, we get

$$(c_3 I_1 + \theta_1 G_1 + c_1 Z_1^t Z_1) \beta_1 + (\rho Z_1^t Z_2) \beta_2 = Z_1^t (c_1 + \rho) Y_{true}, \quad (22)$$

$$(\rho Z_2^t Z_1) \beta_1 + (I_2 + \theta_2 G_2 + c_2 Z_2^t Z_2) \beta_2 = Z_2^t (c_2 + \rho) Y_{true}, \quad (23)$$

where I_1 and I_2 are the identity matrices of the appropriate dimension. Converting into matrix form, we get

$$\begin{bmatrix} c_3 I_1 + \theta_1 G_1 + c_1 Z_1^t Z_1 & \rho Z_1^t Z_2 \\ \rho Z_2^t Z_1 & I_2 + \theta_2 G_2 + c_2 Z_2^t Z_2 \end{bmatrix} \begin{bmatrix} \beta_1 \\ \beta_2 \end{bmatrix} = \begin{bmatrix} Z_1^t (c_1 + \rho) \\ Z_2^t (c_2 + \rho) \end{bmatrix} Y_{true}. \quad (24)$$

$$\begin{bmatrix} \beta_1 \\ \beta_2 \end{bmatrix} = \begin{bmatrix} c_3 I_1 + \theta_1 G_1 + c_1 Z_1^t Z_1 & \rho Z_1^t Z_2 \\ \rho Z_2^t Z_1 & I_2 + \theta_2 G_2 + c_2 Z_2^t Z_2 \end{bmatrix}^{-1} \begin{bmatrix} Z_1^t (c_1 + \rho) \\ Z_2^t (c_2 + \rho) \end{bmatrix} Y_{true}. \quad (25)$$

For a new data point x having representation x_A and x_B w.r.t. *view - A* and *view - B*,

respectively, we give the classification function as follows:

$$class(x) = \arg \max_{i \in \{1,2\}} \{y_{c_i}\}, \quad (26)$$

where

$$y_c = \frac{1}{2} ([x_A \ \phi(x_A W_A + b_A)] \beta_1 + [x_B \ \phi(x_B W_B + b_B)] \beta_2)$$

and $y_c = (y_{c_1}, y_{c_2})$.

where W_A and W_B are the randomly generated weights matrices, and b_A and b_B represents the bias column vectors of the bias matrices B_A and B_B , respectively. Since, all the columns of the bias matrix B_A are identical, hence b_A can be chosen to be any column of B_A . A similar argument follows for b_B . The algorithm for the proposed GRVFL-MV is presented in Algorithm 1.

3.1. LFDA Under the GE Framework

The intrinsic as well as the penalty graphs are constructed using concatenated matrices Z_1 and Z_2 . Specifically, for Z_1 , we have $\mathcal{G}_1^{int} = \{Z_{1,1} \Delta^{int}\}$ and $\mathcal{G}_1^{pen} = \{Z_{1,1} \Delta^{pen}\}$. Similarly for Z_2 , we have $\mathcal{G}_2^{int} = \{Z_{2,2} \Delta^{int}\}$ and $\mathcal{G}_2^{pen} = \{Z_{2,2} \Delta^{pen}\}$. Hence, the intrinsic graph is denoted as $G_{int}^1 = Z_1^t \mathbb{L}_1 Z_1$ and the penalty graph as $G_{pen}^1 = Z_1^t \mathbb{U}_1 Z_1$. Similarly, for Z_2 , the intrinsic graph is $G_{int}^2 = Z_2^t \mathbb{L}_2 Z_2$ and the penalty graph is $G_{pen}^2 = Z_2^t \mathbb{U}_2 Z_2$. Within the graph embedding (GE) framework, we employ the weighting scheme of Local Fisher Discriminant Analysis (LFDA) [39]. Consequently, the weights for the LFDA model's intrinsic and penalty graphs are determined as follows:

$${}_i\Delta_{kl}^{int} = \begin{cases} \frac{\lambda_{kl}}{N_{c_k}}, & c_k = c_l \\ 0, & otherwise. \end{cases} \quad (27)$$

$${}_i\Delta_{kl}^{pen} = \begin{cases} \lambda_{kl}(\frac{1}{N} - \frac{1}{N_{c_k}}), & c_k = c_l \\ \frac{1}{N}, & otherwise. \end{cases} \quad (28)$$

Where $i = 1, 2$. In this context, N_{c_k} denotes the number of samples within the class labeled as c_k , while λ_{kl} quantifies the similarity between z_k and z_l , where $z_k, z_l \in Z_i$ ($i = 1, 2$). The kernel function is utilized in this paper to compute the similarity measure, i.e., $\lambda_{kl} = \exp(\frac{-\|z_k - z_l\|^2}{2\sigma^2})$ where σ is a scaling parameter.

Algorithm 1 GRVFL-MV Model Algorithm

Input: Training datasets X_A and X_B .

Output: GRVFL-MV model.

- 1: Given the values for $c_1, c_2, c_3, \theta_1, \theta_2$, and ρ .
 - 2: Compute Z_1 and Z_2 using Equation (8).
 - 3: Compute intrinsic and penalty graph weights using Equations (27) and (28) for Z_1 and Z_2 .
 - 4: Calculate Laplacian matrices $\mathbb{L}_i = \mathbb{D}_i - {}_i\Delta^{int}$ and $\mathbb{U}_i = \mathbb{L}_i^p = \mathbb{D}_i^p - {}_i\Delta^{pen}$ for Z_i ($i = 1, 2$).
 - 5: Compute $G_{int}^1 = Z_1^t \mathbb{L}_1 Z_1$ and $G_{pen}^1 = Z_1^t \mathbb{U}_1 Z_1$ for Z_1 , and $G_{int}^2 = Z_2^t \mathbb{L}_2 Z_2$ and $G_{pen}^2 = Z_2^t \mathbb{U}_2 Z_2$ for Z_2 .
 - 6: Compute $G_1 = (G_{pen}^1)^{-1} G_{int}^1$ and $G_2 = (G_{pen}^2)^{-1} G_{int}^2$.
 - 7: Use Equation (25) to calculate β_1 and β_2 .
 - 8: Use test condition (26) to classify a new data point.
-

3.2. Computational Complexity

We analyze the computational complexity of our proposed GRVFL-MV model in this section. For X_A , computing the graph embedding (GE) matrix G_1 using the methodologies from [19] which account for intrinsic as well as penalty graph structures results in a time complexity of $\mathcal{O}((m+h_1)^3 + (m+h_1)^2 l)$. Similarly, for X_B , computing G_2 yields a complexity

of $\mathcal{O}((n+h_2)^3+(n+h_2)^2l)$. Thus, the GE process incurs a total computational complexity of $\mathcal{O}((n+h_1)^3+(n+h_1)^2l)+\mathcal{O}((m+h_2)^3+(m+h_2)^2l)$. To solve our model, we address (25). The complexity of this step is primarily governed by the inversion of a square matrix with an order of $(m+n+h_1+h_2)$, leading to a computational complexity of $\mathcal{O}((m+n+h_1+h_2)^3)$. Consequently, the total computational complexity of our proposed model becomes $\mathcal{O}((n+h_1)^3+(n+h_1)^2l)+\mathcal{O}((m+h_2)^3+(m+h_2)^2l)+\mathcal{O}((m+n+h_1+h_2)^3)\approx\mathcal{O}((m+n+h_1+h_2)^3)$.

4. Experiments and Result Discussion

The performance of the proposed model has been evaluated against the baseline models: SVM2K [10], MvTSVM [47], ELM1 (performance of ELM [16] on ‘view – A’), ELM2 (performance of ELM [16] on ‘view – B’), RVFL1 (performance of RVFL [29] on ‘view – A’) and RVFL2 (performance of RVFL [29] on ‘view – B’), and MVLDM [15]. The datasets used for the evaluation are UCI [9], KEEL [8], Animal with Attributes (AwA)¹, and Corel5K².

4.1. Experimental Setup

The experiments are carried out on a PC equipped with an Intel(R) Xeon(R) Gold 6226R processor clocked at 2.90GHz and 128 GB of RAM. The system runs on Windows 11 and uses Python 3.11. The dual of the QPP in SVM2K [10] and MvTSVM [47] is solved using the “QP solvers” function from the CVXOPT package. The dataset is randomly divided, allocating 70% of the samples for training and 30% for testing. Hyperparameters are optimized and validated using a five-fold cross-validation approach. The regularization parameters c_i ($i = 1, 2, 3$), the graph regularization parameters θ_j ($j = 1, 2$), and the coupling parameter ρ are tuned within the range $\{10^{-5}, 10^{-4}, \dots, 10^5\}$. In our experiments,

¹<http://attributes.kyb.tuebingen.mpg.de>

²<https://wang.ist.psu.edu/docs/related/>

we have taken $c_1 = c_2 = c_3$ and $\theta_1 = \theta_2$. All the hyperparameters of the baseline models were also taken within the same range. The hidden neurons (h_l) varies as 3:20:203.

4.2. Experiments on UCI and KEEL Datasets

Table 1: Average Accuracy and Average Rank of the baseline models and the proposed GRVFL-MV model over UCI and KEEL datasets.

Model	SVM2K [10]	MvTSVM [47]	ELM1 [16]	ELM2 [16]	RVFL1 [29]	RVFL2 [29]	MVLDM [15]	GRVFL-MV (proposed)
Average ACC	75.24	65.83	82.11	80.94	82.63	80.26	80.58	84.35
Average Rank	5.52	7.69	4.02	4.30	3.54	4.41	4.80	1.74

Within this subsection, we delve into analyzing the statistical significance of the results obtained from our experiments, specifically concentrating on datasets sourced from UCI and KEEL repositories [9, 8]. Through our assessment, we encompass a total of 27 datasets. Given the absence of inherent multi-view characteristics in the UCI and KEEL datasets, we designated the 95% principal component extracted from the original data as ‘*view – B*’, while the unaltered data itself acts as ‘*view – A*’. In order to thoroughly compare the performance levels between our proposed graph random vector functional link based on the multi-view learning (GRVFL-MV) model and the baseline models with optimized hyperparameters, please refer to Table S.1 in the Supplementary Material. The outcomes illustrated in Table 1 in the paper underline the average accuracy (ACC) and average rank of each model across the UCI and KEEL datasets. The baseline models SVM2K, MvTSVM, ELM1, EML2, RVFL1, RVFL2, and MVLDM achieves the average ACC of 75, 24%, 65.83%, 82.11%, 80.94%, 82.62%, 80.26%, and 80.58%, respectively. The GRVFL-MV model that we put forward exhibited an outstanding average accuracy rate of 84.35%, surpassing the performance levels of the baseline models. The difference in average ACC of the proposed model and the baseline models lies approximately between 4% – 20%. This showcases the superior generalization capabilities inherent in our proposed model compared to the baseline models.

In order to further assess the effectiveness of the proposed model, a ranking method is utilized. This method involves assigning a rank to each model for every dataset, where the model that performs the best is given the lowest rank, and the model that performs the worst is given the highest rank. The average rank for each model is then calculated by finding the mean of its ranks across all datasets. If there are a total of N datasets, each evaluated with λ models, the rank of the p^{th} model on the t^{th} dataset can be represented as s_p^t . Subsequently, the average rank of the p^{th} model is calculated as $R_p = \frac{1}{N} \sum_{t=1}^N s_p^t$. The proposed GRVFL-MV model has been able to achieve an average rank of 1.74. On the other hand, the baseline models such as SVM2K, MvTSVM, ELM1, ELM2, RVFL1, RVFL2, and MVLDM have average ranks of 5.52, 7.69, 4.02, 4.30, 3.54, 4.41, and 4.80, respectively. These results clearly demonstrate the superiority of the proposed model over the baseline models.

In order to assess the statistical significance of the proposed model, the Friedman test is utilized as outlined in [7]. This particular test is designed to pinpoint noteworthy variations among the models being compared by scrutinizing their average ranks. The underlying assumption of the null hypothesis is that all models showcase an identical average rank, indicating an equivalent level of performance. The Friedman test adheres to a chi-squared distribution denoted as χ_F^2 with $(\lambda - 1)$ degrees of freedom, which can be calculated using the formula: $\chi_F^2 = \frac{12N}{\lambda(\lambda+1)} \left[\sum_p R_p^2 - \frac{\lambda(\lambda+1)^2}{4} \right]$. Here, R_p signifies the average rank of the p th model, λ represents the total number of models, and N denotes the number of datasets involved in the analysis. The Friedman statistic F_F is determined by the formula: $F_F = \frac{(N-1)\chi_F^2}{N(\lambda-1)-\chi_F^2}$, where the F -distribution is characterized by $(\lambda - 1)$ and $(\lambda - 1) \times (N - 1)$ degrees of freedom. Given that $N = 27$ and $\lambda = 8$, the values of χ_F^2 and F_F are calculated to be 91.37 and 24.33, respectively. By consulting the F -distribution table at a 5% level of significance (α), the critical value of $F_F(7, 182) = 2.39$ is obtained. Since the calculated value of F_F is 24.33, which exceeds the critical value of 2.39, the

null hypothesis is rejected. This outcome underscores a substantial statistical distinction among the models under comparison.

Table 2: The statistical comparison of the proposed GRVFL-MV model with the baseline models on UCI and KEEL datasets using the Nemenyi post hoc test.

	SVM2K [10]	MvTSVM [47]	ELM1 [16]	ELM2 [16]	RVFL1 [29]	RVFL2 [29]	MVLDM [15]
GRVFL-MV (proposed)	✓	✓	✓	✓	✓	✓	✓

✓ indicates that the model listed in the row is superior to the model mentioned in the column.

In addition, the Nemenyi post hoc test [7] is utilized to delve deeper into the differences between the models. If the average ranks of the models exhibit a variance of at least the critical difference (CD), then they are deemed to be significantly distinct. The CD is determined by the formula: $CD = q_\alpha \left[\frac{\lambda(\lambda+1)}{6N} \right]^{1/2}$. On calculating, we get the $CD = 1.35$. The results presented in Table 2 provide clear evidence that the average rank difference between the baseline model and the proposed GRVFL-MVL is larger than the critical difference (CD) value. To be more precise, the average rank difference between MvTSVM and GRVFL-MV is 5.95, which is greater than the CD value of 1.35. Similarly, the average rank difference between MVLDM and GRVFL-MV is 3.06, also surpassing the CD value. Therefore, these results unequivocally demonstrate that the proposed model exhibits significant dissimilarity compared to the baseline models.

Furthermore, a pairwise win-tie-loss sign test is conducted under the assumption of equal performance between the two models under the null hypothesis. It is anticipated that each model will emerge victorious in roughly half of the total datasets, denoted as $\frac{N}{2}$, where N represents the total number of datasets. To establish statistical significance, a model must secure wins in approximately $\frac{N}{2} + 1.96 \frac{\sqrt{N}}{2}$ datasets more than its counterpart. In scenarios where there is an even number of ties between the models, the ties are evenly distributed. Conversely, in cases of an odd number of ties, one tie is discounted, and the remaining ties are divided between the models. With N set at 27, a minimum of 18.59 wins is required to establish a significant difference between the two models.

Table 3: Pairwise win-tie-loss test of proposed GRVFL-MV model and baseline models on UCI and KEEL datasets.

	SVM2K [10]	MvTSVM [47]	ELM1 [16]	ELM2 [16]	RVFL1 [29]	RVFL2 [29]	Large_Margin [15]
MvTSVM [47]	[2, 2, 23]						
ELM1 [16]	[18, 1, 8]	[27, 0, 0]					
ELM2 [16]	[18, 2, 7]	[26, 0, 1]	[10, 4, 13]				
RVFL1 [29]	[21, 1, 5]	[27, 0, 0]	[11, 10, 6]	[14, 4, 9]			
RVFL2 [29]	[18, 1, 8]	[25, 1, 1]	[9, 5, 13]	[10, 9, 8]	[7, 7, 13]		
Large_Margin [15]	[16, 1, 10]	[24, 0, 3]	[11, 0, 16]	[11, 0, 16]	[9, 0, 18]	[13, 0, 14]	
GRVFL-MV (proposed)	[25, 0, 2]	[27, 0, 0]	[22, 1, 4]	[23, 1, 3]	[21, 1, 5]	[24, 1, 2]	[25, 0, 2]

wherein $[x \ y \ z]$, x signifies no. of wins, y no. of draws, and z no. of losses.

The results depicted in Table 3 showcase a distinct advantage for our proposed model over the baseline model. Clearly, we can see that our proposed model wins on at least 21 (> 18.59) datasets out of 27 datasets. Hence, our proposed model is far superior to the baseline models. In particular, we can observe that our proposed GRVFL-MV surpasses SVM2K in 25 datasets out of the 27 datasets. Furthermore, it outperforms the MvTSVM in all 27 datasets while excelling against MVLDM in 25 datasets out of the 27. The findings unequivocally affirm that our proposed model exhibits a significantly higher performance level compared to the baseline models.

4.3. Experiments on Corel5k Datasets

The Corel5k³ dataset serves as a prominent benchmark in the realms of computer vision and image processing. Comprising 5,000 images across 50 distinct categories, each category includes 100 images. This dataset is widely used for a variety of applications, including content-based image retrieval (CBIR), object recognition, and image classification. We divide the dataset into 50 binary datasets using the one-versus-rest approach. For every binary dataset, 100 photographs from the target category make up the positive class, while another 100 images are chosen at random from the other categories to make up the negative class. This approach facilitates the creation of tailored binary datasets for focused analysis

³<https://wang.ist.psu.edu/docs/related/>

and experimentation.

Table 4: Average Accuracy and Average Rank of the baseline models and the proposed model GRVFL-MV over Corel5k datasets.

Model	SVM2K [10]	MvTSVM [47]	ELM1 [16]	ELM2 [16]	RVFL1 [29]	RVFL2 [29]	MVLDM [15]	GRVFL-MV (proposed)
Average ACC	74.87	49.93	74.98	74.83	76.33	75.43	69.87	77.33
Average Rank	4.11	7.91	3.99	3.97	3.42	4.05	5.61	2.94

The results presented in Table 4 provide clear evidence that our proposed model outperforms the baseline models. With an average accuracy (ACC) of 77.33%, our model achieves the highest accuracy among all the models compared. Additionally, the proposed GRVFL-MV model obtains the lowest average rank of 2.94, indicating its superior performance compared to the baseline models. These findings are from the 50 datasets from Corel5k, which further solidifies the superiority of our proposed model. For more detailed experimental results, please refer to Table S.2 in the supplementary file.

4.4. Experiments on Animal with Attributes (AwA) Datasets

AwA⁴ is a large dataset with 30,475 images covering 50 different animal types. Six representations of pre-extracted features are used to describe each image. For our analysis, we focus on a subset of ten specific test classes drawn from this dataset. These classes include animals like chimpanzees, giant pandas, leopards, Persian cats, pigs, hippopotamuses, humpback whales, raccoons, rats, and seals, totaling 6180 images. For our analysis, we employ two distinct feature representations: a 2000-dimensional L_1 normalized speeded-up robust features (SURF) descriptors (*view - B*) and a 252-dimensional histogram of oriented gradient features (*view - A*). We build and train 45 binary classifiers using the one-against-one method for every possible combination of class pairs in the dataset. The average rank and ACC of our proposed model are displayed in Table 5 in relation to the baseline models. Across the 45 datasets from AwA, our model achieved the highest average accuracy and the lowest average rank. The average ACC of proposed GRVFL-MV is

⁴<http://attributes.kyb.tuebingen.mpg.de>

Table 5: Average Accuracy and Average Rank of the baseline models and the proposed model GRVFL-MV over AWA datasets.

Model	SVM2K [10]	MvTSVM [47]	ELM1 [16]	ELM2 [16]	RVFL1 [29]	RVFL2 [29]	MVLDM [15]	GRVFL-MV (proposed)
Average ACC	77.46	64.31	71.74	75.99	72.87	77.46	73.33	83.29
Average Rank	3.46	6.84	5.99	4.32	5.22	3.59	5.02	1.56

83.29, which is upto 4% to 20% higher than the baseline models. Also, GRVFL-MV has the lowest average rank of 1.56. The results clearly demonstrate the superior performance of the proposed GRVFL-MV model over the baseline models. For more detailed experimental findings, please refer to Table S.3 in the supplementary file.

4.5. Sensitivity Analysis of Hyperparameters C_1 and C_2

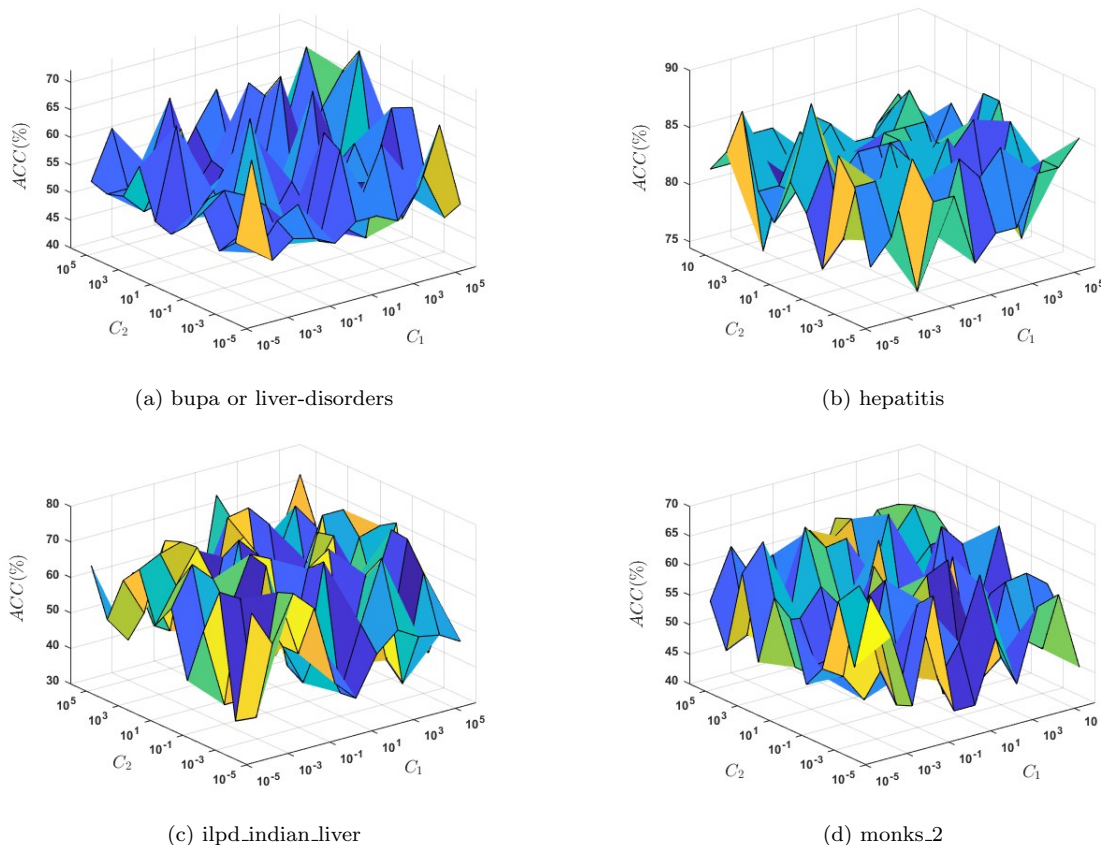


Figure 2: The effect of hyperparameter (c_1, c_2) tuning on the accuracy (ACC) of some UCI and KEEL datasets on the performance of proposed GRVFL-MV model.

To gain a comprehensive understanding of how hyperparameters affect the generaliza-

tion ability of the proposed GRVFL-MV model, we conducted a systematic exploration of the hyperparameter space by tuning the values of c_1 and c_2 . This helps us to identify the optimal configuration that maximizes predictive accuracy and improves the model’s resilience to previously unseen data. Fig. 2. visually represents how the accuracy of the model behaves when the hyperparameters are tuned. The visual clearly shows that the proposed model is highly sensitive to the values of hyperparameters c_1 and c_2 . In Fig. 2. (a), we see that optimal accuracy is achieved when $c_1 = 10^5$ and $c_2 = 10^4$ whereas, in Fig. 2. (c), optimal configuration is found at two distinct coordinates, $(10^5, 10^5)$ and $(10, 10^5)$. Similar observations can be made for Fig. 2. (b) and Fig. 2. (d). Overall, these findings underscore the need for careful selection of hyperparameter values to achieve optimal model performance.

4.6. Sensitivity Analysis of Coupling Parameter ρ

The primal optimization problem (7) combines two distinct classification objectives, each corresponding to a different view. These objectives are linked through a coupling term $\xi_1^t \xi_2$, where ρ serves as the regularization constant known as the coupling parameter. We analyzed the impact of ρ on our model’s performance by fixing other parameters at their optimal values and tuning ρ within the specified range outlined in the experimental setup.

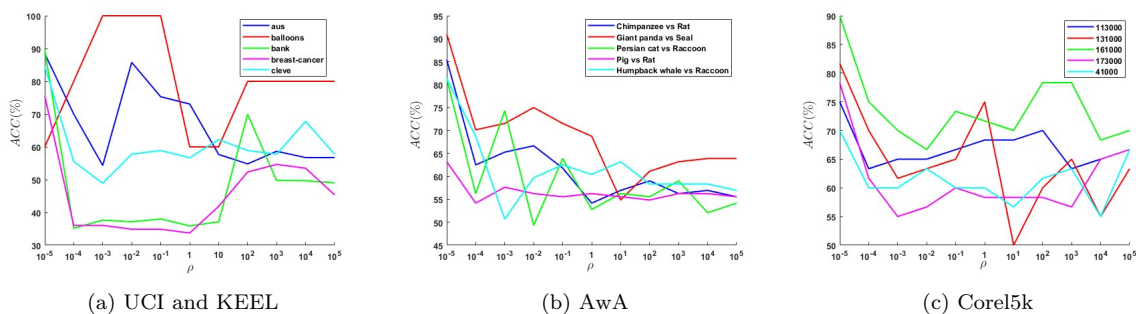


Figure 3: The effect of coupling parameter ρ tuning on the accuracy (ACC) of UCI and KEEL, AWA, and Corel5k datasets on the performance of proposed GRVFL-MV model.

The performance of the proposed model across different datasets is depicted in Fig. 3. It can be observed from Fig. 3. (a) that the proposed GRVFL-MV model achieves the highest accuracy when ρ is set to 10^{-5} . This trend is also evident in Fig.3. (b) and Fig.3. (c). These results indicate that the optimal effect of coupling terms and improved generalization performance are achieved when ρ is tuned to 10^{-5} .

4.7. Sensitivity Analysis of Graph Regularization Parameter θ

The primal optimization problem (7) involves two graph regularization parameters θ_1 and θ_2 for each view, with the goal of preserving the geometrical aspects of multiview data through the graph embedding (GE) framework in the model. In our experiment, we set $\theta_1 = \theta_2 = \theta$ to study the effect of geometrical properties of the multiview data through the LFDA technique under the GE framework.

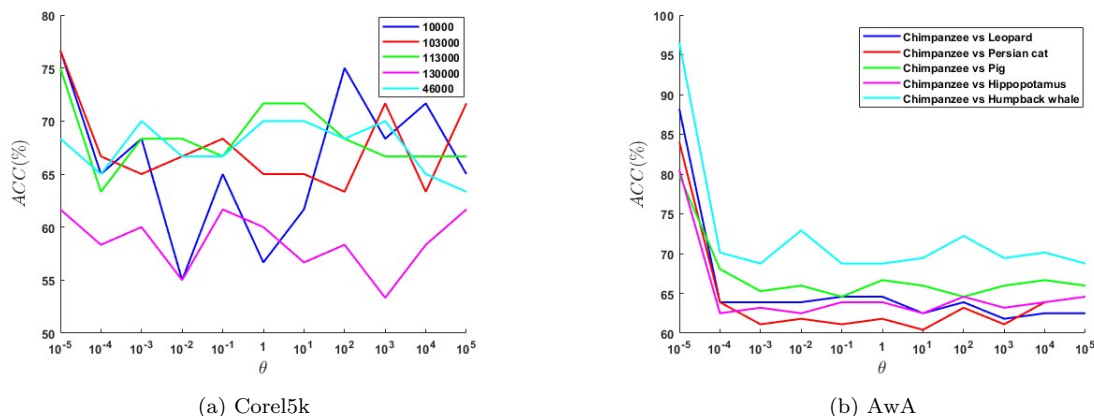


Figure 4: The effect of graph embedding parameter θ tuning on the accuracy (ACC) of Corel5k and AWA datasets on the performance of proposed GRVFL-MV model.

The impact of tuning θ on the efficacy of the GRVFL-MV model is illustrated in Fig. 4. In Fig. 4. (a) when utilizing datasets from Corel5k, it is evident that the model’s performance is most favorable initially at the minimum ρ value, specifically at $\rho = 10^{-5}$, and subsequently performance increases for $\rho > 1$. Conversely, in Fig. 4. (b), the optimal performance is achieved at $\rho = 10^{-5}$ but then experiences a significant decline.

These results emphasize the critical importance of selecting the appropriate ρ value for maximizing the proposed model’s performance.

5. Conclusion

In this study, we presented a generic framework that fuses RVFL architecture with MVL, enhancing generalization by incorporating intrinsic and penalty graphical representations of multiview data via the GE framework, resulting in the development of the GRVFL-MV model. The proposed model aims to enhance the classification performance by fusing information from multiple views. To evaluate the performance of the proposed model, it is compared to various baseline models using UCI and KEEL datasets, Corel5K datasets, and AWA datasets. The experimental results reveal several key findings. Firstly, the proposed GRVFL-MV model demonstrates exceptional performance for UCI and KEEL datasets, achieving an average accuracy improvement ranging from 4% to 20% compared to the baseline models. Moreover, it also achieves the lowest rank among all the models considered. Secondly, in the case of the Corel5K dataset, our proposed GRVFL-MV model outperforms the baseline models by achieving the highest average accuracy and the lowest average rank. This indicates its superior performance in handling the Corel5K dataset. Lastly, for the AWA dataset, the proposed model exhibits outstanding performance by achieving an accuracy improvement of up to 20% compared to the baseline models. Additionally, it also attains the least average rank among all the models considered. Furthermore, a comprehensive statistical analysis is conducted to validate the effectiveness and superiority of the proposed model. The analysis includes a ranking scheme, Friedman test, Nemenyi post hoc test, and win-tie-loss test. The results of these tests unequivocally support the superiority of the proposed GRVFL-MV model over the existing baseline models.

Our proposed models have shown exceptional performance in binary classification tasks

for multi-view datasets. However, their effectiveness in multiclass problems has yet to be evaluated. Future research should focus on adapting these models for multiclass classification. Moreover, an essential research direction involves extending the models to accommodate datasets with more than two views while simultaneously reducing computational complexity.

Acknowledgment

This project is supported by the Indian government through grants from the Department of Science and Technology (DST) and the Ministry of Electronics and Information Technology (MeitY). The funding includes DST/NSM/R&D_HPC_Appl/2021/03.29 for the National Supercomputing Mission and MTR/2021/000787 for the Mathematical Research Impact-Centric Support (MATRICS) scheme. Furthermore, Md Sajid's research fellowship is funded by the Council of Scientific and Industrial Research (CSIR), New Delhi, under the grant 09/1022(13847)/2022-EMR-I. The authors express their gratitude for the resources and support provided by IIT Indore.

References

- [1] W. Cao, X. Wang, Z. Ming, J. Gao, A review on neural networks with random weights, *Neurocomputing* 275 (2018) 278–287.
- [2] W. Cao, P. Yang, Z. Ming, S. Cai, J. Zhang, An improved fuzziness based random vector functional link network for liver disease detection, in: 2020 IEEE 6th Intl Conference on Big Data Security on Cloud (BigDataSecurity), IEEE Intl Conference on High Performance and Smart Computing,(HPSC) and IEEE Intl Conference on Intelligent Data and Security (IDS), IEEE, pp. 42–48.
- [3] T. Chakravorti, P. Satyanarayana, Non linear system identification using kernel based

- exponentially extended random vector functional link network, *Applied Soft Computing* 89 (2020) 106117.
- [4] N. Chen, J. Zhu, E. Xing, Predictive subspace learning for multi-view data: a large margin approach, *Advances in Neural Information Processing Systems* 23 (2010).
- [5] W. Cui, L. Zhang, B. Li, J. Guo, W. Meng, H. Wang, L. Xie, Received signal strength based indoor positioning using a random vector functional link network, *IEEE Transactions on Industrial Informatics* 14 (2017) 1846–1855.
- [6] W. Dai, Y. Ao, L. Zhou, P. Zhou, X. Wang, Incremental learning paradigm with privileged information for random vector functional-link networks: Irvfl+, *Neural Computing and Applications* 34 (2022) 6847–6859.
- [7] J. Demšar, Statistical comparisons of classifiers over multiple data sets, *The Journal of Machine Learning Research* 7 (2006) 1–30.
- [8] J. Derrac, S. Garcia, L. Sanchez, F. Herrera, KEEL data-mining software tool: Data set repository, integration of algorithms and experimental analysis framework, *Journal of Multiple-Valued Logic and Soft Computing* 17 (2015) 255–287.
- [9] D. Dua, C. Graff, UCI machine learning repository., Available: <http://archive.ics.uci.edu/ml> (2017).
- [10] J. Farquhar, D. Hardoon, H. Meng, J. Shawe-Taylor, S. Szepesvári, Two view learning: Svm-2k, theory and practice, *Advances in Neural Information Processing Systems* 18 (2005).
- [11] M.A. Ganaie, M. Sajid, A.K. Malik, M. Tanveer, Graph embedded intuitionistic fuzzy random vector functional link neural network for class imbalance learning, *IEEE Transactions on Neural Networks and Learning Systems* (2024) 1–10.

- [12] M. Gori, A. Tesi, On the problem of local minima in backpropagation, *IEEE Transactions on Pattern Analysis and Machine Intelligence* 14 (1992) 76–86.
- [13] B. Gülmez, Stock price prediction with optimized deep lstm network with artificial rabbits optimization algorithm, *Expert Systems with Applications* 227 (2023) 120346.
- [14] L. Houthuys, R. Langone, J.A. Suykens, Multi-view least squares support vector machines classification, *Neurocomputing* 282 (2018) 78–88.
- [15] K. Hu, Y. Xiao, W. Zheng, W. Zhu, C.H. Hsu, Multiview large margin distribution machine, *IEEE Transactions on Neural Networks and Learning Systems* (2024).
- [16] G.B. Huang, Q.Y. Zhu, C.K. Siew, Extreme learning machine: theory and applications, *Neurocomputing* 70 (2006) 489–501.
- [17] T. Hussain, K. Muhammad, W. Ding, J. Lloret, S.W. Baik, V.H.C. de Albuquerque, A comprehensive survey of multi-view video summarization, *Pattern Recognition* 109 (2021) 107567.
- [18] B. IgelNIK, Y.H. Pao, Stochastic choice of basis functions in adaptive function approximation and the functional-link net, *IEEE Transactions on Neural Networks and Learning Systems* 6 (1995) 1320–1329.
- [19] A. Iosifidis, A. Tefas, I. Pitas, Graph embedded extreme learning machine, *IEEE Transactions on Cybernetics* 46 (2015) 311–324.
- [20] R.A. Jacobs, Increased rates of convergence through learning rate adaptation, *Neural Networks* 1 (1988) 295–307.
- [21] M. Kan, S. Shan, H. Zhang, S. Lao, X. Chen, Multi-view discriminant analysis, *IEEE Transactions on Pattern Analysis and Machine Intelligence* 38 (2015) 188–194.

- [22] M.J. Kearns, U. Vazirani, An introduction to computational learning theory, MIT press, 1994.
- [23] J. Li, Y. Wu, J. Zhao, K. Lu, Low-rank discriminant embedding for multiview learning, *IEEE Transactions on Cybernetics* 47 (2016) 3516–3529.
- [24] X. Li, Y. Yang, N. Hu, Z. Cheng, J. Cheng, Discriminative manifold random vector functional link neural network for rolling bearing fault diagnosis, *Knowledge-Based Systems* 211 (2021) 106507.
- [25] C. Liu, Y. Wang, D. Li, X. Wang, Domain-incremental learning without forgetting based on random vector functional link networks, *Pattern Recognition* 151 (2024) 110430.
- [26] A. Malik, R. Gao, M. Ganaie, M. Tanveer, P.N. Suganthan, Random vector functional link network: Recent developments, applications, and future directions, *Applied Soft Computing* 143 (2023) 110377.
- [27] A. Malik, M. Tanveer, Graph embedded ensemble deep randomized network for diagnosis of alzheimer’s disease, *IEEE/ACM Transactions on Computational Biology and Bioinformatics* (2022) 1–13.
- [28] A.K. Malik, M. Ganaie, M. Tanveer, Graph embedded intuitionistic fuzzy weighted random vector functional link network, in: *2022 IEEE Symposium Series on Computational Intelligence (SSCI)*, IEEE, pp. 293–299.
- [29] Y.H. Pao, G.H. Park, D.J. Sobajic, Learning and generalization characteristics of the random vector functional-link net, *Neurocomputing* 6 (1994) 163–180.
- [30] R. Pilli, T. Goel, R. Murugan, M. Tanveer, P.N. Suganthan, Kernel ridge regression-

- based randomized network for brain age classification and estimation, *IEEE Transactions on Cognitive and Developmental Systems* (2024) 1–10.
- [31] A. Quadir, M. Akhtar, M. Tanveer, Enhancing multiview synergy: Robust learning by exploiting the wave loss function with consensus and complementarity principles, arXiv preprint arXiv:2408.06819 (2024).
- [32] A. Quadir, M. Sajid, M. Tanveer, Multiview random vector functional link network for predicting DNA-binding proteins, arXiv preprint arXiv:2409.02588 (2024).
- [33] A. Quadir, M. Tanveer, Multiview learning with twin parametric margin SVM, *Neural Networks* 180 (2024) 106598.
- [34] M. Sajid, A.K. Malik, M. Tanveer, Intuitionistic fuzzy broad learning system: Enhancing robustness against noise and outliers, *IEEE Transactions on Fuzzy Systems* 32 (2024) 4460–4469.
- [35] M. Sajid, A.K. Malik, M. Tanveer, P.N. Suganthan, Neuro-fuzzy random vector functional link neural network for classification and regression problems, *IEEE Transactions on Fuzzy Systems* 32 (2024) 2738–2749.
- [36] W. Schmidt, M. Kraaijveld, R. Duin, Feedforward neural networks with random weights, in: *Proceedings., 11th IAPR International Conference on Pattern Recognition. Vol.II. Conference B: Pattern Recognition Methodology and Systems*, pp. 1–4.
- [37] M. Shafiq, Z. Gu, Deep residual learning for image recognition: A survey, *Applied Sciences* 12 (2022) 8972.
- [38] P.N. Suganthan, R. Katuwal, On the origins of randomization-based feedforward neural networks, *Applied Soft Computing* 105 (2021) 107239.

- [39] M. Sugiyama, Dimensionality reduction of multimodal labeled data by local fisher discriminant analysis., *Journal of Machine Learning Research* 8 (2007).
- [40] J. Sun, H. Fujita, Y. Zheng, W. Ai, Multi-class financial distress prediction based on support vector machines integrated with the decomposition and fusion methods, *Information Sciences* 559 (2021) 153–170.
- [41] C. Tang, X. Liu, X. Zhu, E. Zhu, Z. Luo, L. Wang, W. Gao, Cgd: Multi-view clustering via cross-view graph diffusion, in: *Proceedings of the AAAI conference on Artificial Intelligence*, volume 34, pp. 5924–5931.
- [42] C. Tang, X. Zhu, X. Liu, M. Li, P. Wang, C. Zhang, L. Wang, Learning a joint affinity graph for multiview subspace clustering, *IEEE Transactions on Multimedia* 21 (2018) 1724–1736.
- [43] M. Tanveer, M.A. Ganaie, I. Beheshti, T. Goel, N. Ahmad, K.T. Lai, K. Huang, Y.D. Zhang, J. Del Ser, C.T. Lin, Deep learning for brain age estimation: A systematic review, *Information Fusion* 96 (2023) 130–143.
- [44] M. Tanveer, T. Goel, R. Sharma, A.K. Malik, I. Beheshti, J. Del Ser, P.N. Suganthan, C.T. Lin, Ensemble deep learning for Alzheimer’s disease characterization and estimation, *Nature Mental Health* 2 (2024) 655–667, [10.1038/s44220-024-00237-x](https://doi.org/10.1038/s44220-024-00237-x).
- [45] M. Tanveer, M. Sajid, M. Akhtar, A. Quadir, T. Goel, A. Aimen, S. Mitra, Y.D. Zhang, C. Lin, J.D. Ser, Fuzzy deep learning for the diagnosis of alzheimer’s disease: Approaches and challenges, *IEEE Transactions on Fuzzy Systems* (2024) 1–20, [10.1109/TFUZZ.2024.3409412](https://doi.org/10.1109/TFUZZ.2024.3409412).
- [46] X. Xie, Y. Li, S. Sun, Deep multi-view multiclass twin support vector machines, *Information Fusion* 91 (2023) 80–92.

- [47] X. Xie, S. Sun, Multi-view twin support vector machines, *Intelligent Data Analysis* 19 (2015) 701–712.
- [48] J. Xu, J. Han, F. Nie, X. Li, Re-weighted discriminatively embedded k -means for multi-view clustering, *IEEE Transactions on Image Processing* 26 (2017) 3016–3027.
- [49] M. Xu, Understanding graph embedding methods and their applications, *SIAM Review* 63 (2021) 825–853.
- [50] R. Xu, H. Wang, Multi-view learning with privileged weighted twin support vector machine, *Expert Systems with Applications* 206 (2022) 117787.
- [51] S. Yan, D. Xu, B. Zhang, H.J. Zhang, Q. Yang, S. Lin, Graph embedding and extensions: A general framework for dimensionality reduction, *IEEE Transactions on Pattern Analysis and Machine Intelligence* 29 (2006) 40–51.
- [52] T. Yao, Z. Wang, Z. Xie, J. Gao, D.D. Feng, Learning universal multiview dictionary for human action recognition, *Pattern Recognition* 64 (2017) 236–244.
- [53] Q. Ye, P. Huang, Z. Zhang, Y. Zheng, L. Fu, W. Yang, Multiview learning with robust double-sided twin svm, *IEEE Transactions on Cybernetics* 52 (2021) 12745–12758.
- [54] L. Zhang, P.N. Suganthan, A survey of randomized algorithms for training neural networks, *Information Sciences* 364 (2016) 146–155.
- [55] P.B. Zhang, Z.X. Yang, A new learning paradigm for random vector functional-link network: Rvfl+, *Neural Networks* 122 (2020) 94–105.
- [56] X. Zhang, Y. Yang, T. Li, Y. Zhang, H. Wang, H. Fujita, CMC: a consensus multi-view clustering model for predicting alzheimer’s disease progression, *Computer Methods and Programs in Biomedicine* 199 (2021) 105895.

- [57] Y. Zhang, J. Wu, Z. Cai, B. Du, S.Y. Philip, An unsupervised parameter learning model for rvfl neural network, *Neural Networks* 112 (2019) 85–97.
- [58] Z. Zhang, X. Wei, X. Zheng, D.D. Zeng, Predicting product adoption intentions: An integrated behavioral model-inspired multiview learning approach, *Information & Management* 58 (2021) 103484.
- [59] J. Zhao, X. Xie, X. Xu, S. Sun, Multi-view learning overview: Recent progress and new challenges, *Information Fusion* 38 (2017) 43–54.

Table S.2: Performance comparison of the proposed GRVFL-MV along with the baseline models based on classification accuracy for Corel5k datasets.

Dataset	SVM2K [10] (C_1)	MvTSMV [47] (C_1, C_2, D)	ELM1 [16] (C, N)	ELM2 [16] (C, N)	RVFL1 [29] (C, N)	RVFL2 [29] (C, N)	MVLDM [15] ($C_1, \nu_1, \nu_2, \sigma$)	GRVFL-MV [†] (C_1, θ, ρ, N)
1000	81.67 (0.0625)	50 (0.00001, 0.00001, 0.00001)	83.33 (0.0001, 183)	78.33 (0.00001, 43)	83.33 (0.0001, 183)	76.67 (0.00001, 3)	73.33 (0.01, 0.001, 0.001, 4)	83.33 (0.01, 10, 0.001, 23)
10000	71.67 (0.03125)	48.33 (0.00001, 0.00001, 0.00001)	56.67 (1000, 23)	63.33 (1000, 23)	71.67 (0.01, 3)	71.67 (0.00001, 63)	55 (0.01, 0.01, 0.001, 4)	65.00 (1, 10, 0.01, 183)
100000	71.67 (0.0625)	55 (0.00001, 0.00001, 0.00001)	63.33 (100000, 183)	73.33 (0.00001, 123)	78.33 (0.001, 183)	75 (0.00001, 123)	61.67 (100, 1000, 100, 4)	78.33 (0.1, 100, 0.01, 3)
101000	66.67 (0.0625)	58.33 (0.00001, 0.00001, 0.00001)	75 (0.001, 123)	73.33 (0.00001, 143)	75 (0.001, 3)	76.67 (0.00001, 143)	55 (100, 10, 100, 4)	80.00 (1000, 10000, 10, 23)
102000	81.67 (0.03125)	51.67 (0.00001, 0.00001, 0.00001)	81.67 (0.01, 63)	75 (0.00001, 143)	71.67 (0.01, 3)	71.67 (100000, 3)	83.33 (0.001, 0.001, 0.0001, 4)	81.67 (0.1, 100, 0.00001, 3)
103000	73.33 (0.03125)	45 (0.00001, 0.00001, 0.00001)	80 (0.001, 163)	75 (0.0001, 43)	81.67 (0.001, 163)	73.33 (0.00001, 43)	65 (0.0001, 0.1, 0.001, 4)	80.00 (1000, 100000, 0.0001, 43)
104000	71.67 (32)	46.67 (0.00001, 0.00001, 0.00001)	55 (10, 123)	65 (10000, 23)	76.67 (0.0001, 203)	76.67 (0.00001, 83)	46.67 (0.0001, 0.0001, 0.00001, 4)	51.67 (100, 0.1, 1000, 83)
108000	80 (8)	48.33 (0.00001, 0.00001, 0.00001)	75.65 (0.001, 63)	76.67 (0.00001, 83)	78.33 (0.1, 3)	76.67 (0.00001, 3)	78.33 (100, 1000, 10000, 4)	81.67 (100, 100000, 0.01, 23)
109000	65 (1)	43.33 (0.00001, 0.00001, 0.00001)	68.33 (0.0001, 203)	73.33 (100, 63)	68.33 (0.0001, 203)	75 (0.0001, 43)	73.33 (0.001, 0.001, 0.0001, 0.25)	88.33 (1, 100, 0.001, 23)
113000	66.67 (0.03125)	45 (0.00001, 0.00001, 0.00001)	68.33 (0.001, 123)	63.33 (1000, 203)	70 (0.001, 123)	70 (0.0001, 23)	66.67 (0.0001, 0.001, 0.001, 0.25)	66.67 (100000, 10000, 0.00001, 3)
118000	58.33 (32)	48.33 (0.00001, 0.00001, 0.00001)	68.33 (0.001, 103)	61.67 (100000, 43)	68.33 (0.001, 103)	56.67 (1000, 43)	58.33 (0.01, 0.1, 0.01, 4)	60.00 (10000, 100, 1, 183)
119000	71.33 (16)	53.33 (0.00001, 0.00001, 0.00001)	81.67 (0.001, 143)	83.33 (0.00001, 123)	78.33 (0.01, 63)	80 (0.00001, 83)	70 (0.001, 0.001, 0.01, 0.25)	80.00 (0.0001, 0.01, 0.00001, 23)
12000	60 (32)	48.33 (0.00001, 0.00001, 0.00001)	63.33 (0.0001, 83)	58.33 (0.00001, 63)	63.33 (0.0001, 83)	51.67 (0.00001, 43)	61.67 (0.1, 0.1, 0.1, 2)	68.33 (0.00001, 10000, 1000, 203)
120000	73.33 (0.03125)	48.33 (0.00001, 0.00001, 0.00001)	78.33 (0.01, 203)	80 (0.00001, 203)	78.33 (0.01, 203)	85 (0.00001, 103)	66.67 (0.001, 0.0001, 0.001, 4)	75.00 (0.0001, 10, 100, 203)
121000	63.33 (2)	55 (0.00001, 0.00001, 0.00001)	68.33 (0.0001, 163)	75 (0.00001, 103)	71.67 (0.0001, 103)	71.67 (0.00001, 103)	75.00 (0.001, 0.1, 0.01, 2)	75.00 (0.0001, 0.01, 0.00001, 3)
122000	78.33 (0.0625)	55 (0.00001, 0.00001, 0.00001)	70 (0.01, 163)	76.67 (100, 23)	76.67 (0.01, 163)	71.67 (0.00001, 123)	61.67 (0.01, 0.001, 0.01, 0.25)	81.67 (0.00001, 0.01, 0.0001, 23)
13000	85 (32)	50 (0.00001, 0.00001, 0.00001)	83.33 (0.001, 183)	91.67 (0.00001, 103)	85 (0.001, 183)	90 (0.00001, 43)	78.33 (0.01, 0.001, 0.0001, 2)	85 (0.0001, 0.001, 0.00001, 3)
130000	58.96 (0.03125)	48.33 (0.00001, 0.00001, 0.00001)	58.33 (0.001, 103)	65 (100, 23)	58.33 (0.001, 103)	61.67 (0.00001, 23)	60 (0.001, 0.001, 0.001, 4)	61.67 (0.001, 0.1, 0.00001, 83)
131000	78.33 (0.03125)	63.33 (0.00001, 0.00001, 0.00001)	73.33 (0.001, 163)	76.67 (0.00001, 83)	76.67 (0.01, 23)	83.33 (0.00001, 183)	73.33 (0.01, 0.001, 0.01, 4)	73.33 (1, 1000, 1000, 163)
140000	71.67 (0.0625)	40 (0.00001, 0.00001, 0.00001)	58.33 (0.1, 183)	76.67 (0.00001, 143)	56.67 (0.1, 3)	78.33 (100, 3)	45 (0.01, 0.001, 0.0001, 4)	80.00 (10, 1, 1, 3)
142000	86.67 (0.25)	51.67 (0.00001, 0.00001, 0.00001)	85 (0.001, 183)	68.33 (10000, 23)	91.67 (0.1, 3)	88.33 (1, 3)	78.33 (0.01, 0.001, 0.0001, 4)	91.67 (1, 100, 0.01, 3)
143000	66.67 (0.03125)	51.67 (0.00001, 0.00001, 0.00001)	63.33 (0.001, 163)	65 (0.00001, 203)	63.33 (0.001, 163)	65 (0.00001, 203)	71.67 (0.01, 0.1, 0.1, 0.25)	58.33 (0.001, 10, 1, 183)
144000	73.33 (16)	48.33 (0.00001, 0.00001, 0.00001)	68.33 (0.01, 63)	71.67 (0.00001, 203)	68.33 (0.01, 63)	70 (0.00001, 203)	66.67 (0.1, 0.1, 0.1, 0.25)	68.33 (100, 0.1, 0.00001, 203)
147000	58.33 (0.125)	55 (0.00001, 0.00001, 0.00001)	63.33 (0.01, 203)	73.33 (0.00001, 123)	63.33 (0.01, 203)	73.33 (0.00001, 123)	70 (0.001, 0.001, 0.1, 4)	75.00 (0.1, 1, 0.00001, 203)
148000	86.67 (2)	50 (0.00001, 0.00001, 0.00001)	90 (0.001, 103)	80 (0.00001, 83)	88.33 (0.001, 23)	86.67 (0.00001, 63)	83.33 (0.001, 0.0001, 0.1, 4)	83.33 (0.1, 100, 0.001, 83)
152000	56.67 (0.25)	48.33 (0.00001, 0.00001, 0.00001)	65 (0.00001, 143)	66.67 (0.1, 23)	66.67 (0.00001, 103)	45 (1, 103)	51.67 (0.1, 0.1, 0.001, 0.25)	68.33 (100, 10000, 10, 43)
153000	79.33 (0.5)	55 (0.00001, 0.00001, 0.00001)	76.67 (0.001, 203)	73.33 (0.00001, 43)	76.67 (0.001, 203)	88.33 (0.00001, 43)	80.00 (0.01, 10, 100, 4)	75.00 (1, 1000, 0.1, 203)
161000	86.67 (0.5)	46.67 (0.00001, 0.00001, 0.00001)	91.67 (0.001, 183)	91.67 (0.00001, 143)	88.33 (0.1, 23)	90 (0.00001, 43)	93.33 (0.001, 0.0001, 0.00001, 2)	91.67 (100, 1000, 0.001, 3)
163000	80 (4)	41.67 (0.00001, 0.00001, 0.00001)	80 (0.0001, 203)	78.33 (1, 23)	80 (0.001, 83)	85 (0.00001, 3)	71.67 (0.001, 0.0001, 0.00001, 0.5)	83.33 (0.0001, 0.01, 0.00001, 43)
17000	83.33 (2)	56.67 (0.00001, 0.00001, 0.00001)	86.67 (0.001, 163)	90 (0.00001, 143)	86.67 (0.001, 163)	86.67 (0.00001, 203)	83.33 (0.001, 0.00001, 0.1, 4)	93.33 (0.001, 0.1, 0.0001, 203)
171000	88.33 (0.03125)	48.33 (0.00001, 0.00001, 0.00001)	76.67 (0.001, 123)	68.33 (0.00001, 83)	76.67 (0.001, 123)	75 (0.00001, 3)	63.33 (0.1, 0.001, 0.1, 0.25)	75.00 (0.00001, 0.01, 0.00001, 183)
173000	85 (0.125)	61.67 (0.00001, 0.00001, 0.00001)	86.67 (0.001, 203)	71.67 (1000, 23)	83.33 (0.001, 63)	78.33 (1000, 3)	80 (0.0001, 0.01, 0.1, 0.25)	86.67 (10, 10000, 0.00001, 23)
174000	81.67 (0.03125)	45 (0.00001, 0.00001, 0.00001)	81.67 (0.01, 103)	85 (0.001, 43)	83.33 (0.01, 103)	88.33 (0.00001, 23)	88.33 (0.0001, 0.01, 0.0001, 4)	90.00 (0.00001, 0.0001, 0.00001, 3)
182000	76.67 (0.03125)	46.67 (0.00001, 0.00001, 0.00001)	78.33 (0.001, 183)	76.67 (0.00001, 123)	80 (0.001, 183)	76.67 (0.00001, 123)	70 (0.00001, 0.0001, 0.0001, 0.25)	81.67 (1, 100, 0.1, 3)
183000	70 (4)	48.33 (0.00001, 0.00001, 0.00001)	80 (0.001, 203)	68.33 (1000, 43)	88.33 (0.0001, 203)	80 (0.00001, 43)	68.33 (0.00001, 0.01, 0.00001, 4)	80.00 (1, 10000, 0.0001, 203)
187000	83.33 (0.03125)	43.33 (0.00001, 0.00001, 0.00001)	81.67 (0.0001, 103)	80 (10000, 23)	83.33 (0.001, 103)	85 (0.00001, 3)	81.67 (0.01, 0.01, 0.01, 0.25)	83.33 (0.0001, 0.1, 0.00001, 163)
189000	76.67 (0.25)	58.33 (0.00001, 0.00001, 0.00001)	80 (0.001, 203)	81.67 (0.00001, 123)	80 (0.001, 203)	75 (0.00001, 163)	73.33 (0.01, 0.001, 0.001, 4)	75.00 (1000, 0.1, 10, 3)
20000	65 (0.03125)	40 (0.00001, 0.00001, 0.00001)	63.33 (0.001, 183)	73.33 (100000, 23)	70 (0.01, 3)	63.33 (0.00001, 163)	65 (0.001, 0.001, 0.0001, 4)	73.33 (0.1, 100, 0.00001, 43)
201000	86.67 (1)	58.33 (0.00001, 0.00001, 0.00001)	90 (1, 23)	88.33 (0.00001, 63)	91.67 (0.0001, 63)	80 (0.00001, 23)	80 (0.0001, 0.01, 0.001, 4)	90.00 (0.001, 0.01, 0.00001, 23)
21000	90 (1)	50 (0.00001, 0.00001, 0.00001)	93.33 (0.001, 183)	83.33 (0.00001, 43)	88.33 (0.01, 163)	86.67 (0.00001, 103)	86.67 (0.1, 0.1, 0.1, 0.25)	88.33 (1000, 100000, 0.00001, 203)
22000	70 (0.03125)	46.67 (0.00001, 0.00001, 0.00001)	70 (0.001, 143)	53.33 (1, 23)	73.33 (0.1, 23)	68.33 (0.00001, 43)	68.33 (0.001, 0.001, 0.001, 0.25)	73.33 (10, 1000, 0.001, 203)
231000	65 (0.0625)	55 (0.00001, 0.00001, 0.00001)	61.67 (0.1, 123)	60 (0.00001, 203)	56.67 (0.01, 83)	60 (0.00001, 203)	53.33 (0.1, 0.001, 0.0001, 0.25)	53.33 (100, 1000, 0.0001, 123)
276000	78.67 (0.25)	56.67 (0.00001, 0.00001, 0.00001)	78.33 (0.01, 63)	76.67 (0.00001, 183)	80 (0.01, 63)	76.67 (0.00001, 183)	71.67 (0.001, 0.0001, 0.0001, 4)	78.33 (0.01, 10, 0.0001, 23)
296000	78.33 (16)	46.67 (0.00001, 0.00001, 0.00001)	85 (0.001, 183)	71.67 (0.00001, 103)	85 (0.001, 183)	78.33 (0.00001, 3)	68.33 (0.00001, 0.001, 0.01, 4)	76.67 (0.01, 10, 0.001, 103)
33000	83.33 (0.03125)	43.33 (0.00001, 0.00001, 0.00001)	86.67 (0.001, 143)	81.67 (0.00001, 43)	88.33 (0.01, 3)	81.67 (0.00001, 43)	68.33 (0.01, 0.1, 0.1, 0.25)	88.33 (1, 10000, 0.1, 63)
335000	78.33 (8)	43.33 (0.00001, 0.00001, 0.00001)	75 (0.001, 203)	78.33 (0.00001, 43)	73.33 (0.01, 3)	75 (0.00001, 43)	70 (0.1, 0.1, 0.1, 4)	76.67 (0.00001, 1, 3, 0.0001, 103)
34000	80.33 (0.25)	53.33 (0.00001, 0.00001, 0.00001)	76.67 (0.001, 83)	86.67 (0.00001, 163)	83.33 (0.001, 203)	86.67 (0.00001, 163)	73.33 (0.1, 0.001, 0.001, 0.5)	85.00 (10000, 10000, 1, 3)
384000	85 (8)	55 (0.00001, 0.00001, 0.00001)	78.33 (0.001, 83)	86.67 (1000, 63)	78.33 (0.001, 83)	85 (0.00001, 183)	78.33 (0.01, 0.001, 0.001, 2)	81.67 (0.00001, 0.01, 0.00001, 143)
41000	65 (0.125)	43.33 (0.00001, 0.00001, 0.00001)	66.67 (0.1, 43)	68.33 (0.00001, 183)	56.67 (0.1, 43)	65 (1000, 23)	56.67 (0.001, 0.0001, 0.01, 4)	66.67 (0.00001, 0.01, 0.00001, 143)
46000	70 (0.125)	46.67 (0.00001, 0.00001, 0.00001)	78.33 (0.001, 163)	81.67 (0.00001, 43)	80 (0.001, 163)	83.33 (0.00001, 43)	65 (0.0001, 0.001, 0.01, 4)	71.67 (1000, 100000, 0.00001, 103)
Average ACC	74.87	49.93	74.98	74.83	76.33	75.43	69.87	77.33
Average Rank	4.11	7.91	3.99	3.97	3.42	4.05	5.61	2.94

[†] represents the proposed model.

Table S.3: Performance comparison of the proposed GRVFL-MV along with the baseline models based on classification accuracy for AWA datasets.

Dataset	SVM2K [10] (C_1)	MvTSVM [47] (C_1, C_2, D)	ELM1 [16] (C, N)	ELM2 [16] (C, N)	RVFL1 [29] (C, N)	RVFL2 [29] (C, N)	MVLDM [15] ($C_1, \nu_1, \nu_2, \sigma$)	GRVFL-MV [†] (C_1, θ, ρ, N)
Chimpanzee vs Giant panda	84.03 (0.0001)	47.22 (0.0001, 0.00001, 0.00001)	71.53 (0.0001, 123)	72.92 (0.00001, 163)	71.53 (0.001, 3)	80.89 (0.001, 3)	72.22 (1000, 0.0001, 0.01, 4)	90.97 (0.001, 10, 0.00001, 3)
Chimpanzee vs Leopard	80.11 (0.00001)	46.53 (0.00001, 0.00001, 0.00001)	63.89 (1000, 43)	83.33 (0.00001, 203)	72.92 (0.01, 23)	80.42 (0.0001, 3)	68.75 (0.001, 0.00001, 0.00001, 4)	89.58 (0.001, 100000, 0.00001, 3)
Chimpanzee vs Persian cat	70.86 (0.0001)	50 (0.00001, 0.00001, 0.00001)	79.86 (0.0001, 183)	69.44 (0.00001, 183)	79.17 (0.0001, 183)	80.56 (0.1, 3)	86.11 (100, 0.0001, 0.00001, 4)	83.33 (10, 10000, 0.00001, 3)
Chimpanzee vs Pig	50.42 (0.01)	51.39 (0.00001, 0.00001, 0.00001)	68.75 (0.00001, 163)	81.25 (0.00001, 163)	69.44 (0.00001, 163)	79.17 (10, 3)	66.67 (100000, 0.001, 0.001, 4)	83.33 (0.001, 10, 0.0001, 3)
Chimpanzee vs Hippopotamus	70.94 (0.00001)	54.86 (0.00001, 0.00001, 0.00001)	71.53 (0.00001, 143)	70.14 (0.00001, 183)	72.92 (0.00001, 143)	78.47 (0.001, 3)	78.47 (1000, 0.0001, 1, 4)	78.47 (0.0001, 10, 0.00001, 3)
Chimpanzee vs Humpback whale	92.36 (0.1)	81.39 (0.00001, 0.00001, 0.00001)	86.81 (0.0001, 83)	92.36 (0.00001, 183)	88.89 (0.0001, 83)	91.14 (0.01, 3)	81.25 (10000, 0.001, 0.0001, 4)	96.53 (0.001, 100000, 0.001, 23)
Chimpanzee vs Raccoon	80.33 (0.001)	63.47 (0.00001, 0.00001, 100000)	69.44 (0.0001, 203)	63.89 (0.00001, 123)	73.61 (0.001, 3)	79.86 (1000, 23)	72.22 (10000, 0.00001, 0.01, 4)	83.33 (0.001, 1, 0.0001, 3)
Chimpanzee vs Rat	77.08 (10)	52.78 (0.00001, 0.00001, 0.00001)	57.64 (100000, 43)	75 (0.00001, 183)	63.89 (0.001, 163)	71.94 (0.001, 3)	68.06 (100000, 0.0001, 0.00001, 4)	82.64 (0.1, 1000, 0.0001, 43)
Chimpanzee vs Seal	70.69 (0.01)	53.47 (0.00001, 0.00001, 0.00001)	79.17 (0.0001, 183)	76.39 (0.00001, 143)	79.17 (0.001, 3)	79.81 (0.0001, 3)	75.69 (0.001, 0.001, 0.01, 0.25)	85.42 (0.001, 100000, 0.01, 3)
Giant panda vs Leopard	80.19 (0.01)	54.17 (0.00001, 0.00001, 0.00001)	61.11 (0.0001, 103)	78.47 (0.00001, 203)	72.92 (0.001, 3)	80.11 (0.001, 3)	61.81 (100000, 0.00001, 0.01, 0.25)	90.97 (0.001, 10, 0.001, 3)
Giant panda vs Persian cat	81.81 (0.0001)	52.08 (0.00001, 0.00001, 0.00001)	77.78 (100, 103)	76.39 (0.00001, 203)	64.58 (0.001, 23)	80.42 (100000, 3)	66.67 (0.01, 0.00001, 0.01, 4)	84.03 (0.1, 1000, 0.01, 23)
Giant panda vs Pig	80.56 (0.0001)	51.39 (0.00001, 0.00001, 0.00001)	63.89 (1, 43)	75 (0.00001, 203)	65.97 (0.001, 3)	79.81 (0.001, 3)	65.97 (1000, 0.00001, 0.01, 0.25)	88.19 (0.001, 10, 0.00001, 3)
Giant panda vs Hippopotamus	77.78 (0.01)	54.17 (0.00001, 0.00001, 0.00001)	74.31 (0.00001, 183)	81.25 (0.00001, 183)	68.06 (0.01, 3)	71.94 (0.01, 23)	74.31 (100000, 0.001, 100, 2)	84.72 (0.01, 100, 0.001, 23)
Giant panda vs Humpback whale	93.06 (0.00001)	46.53 (0.00001, 0.00001, 0.00001)	93.06 (0.0001, 203)	91.67 (0.00001, 203)	93.06 (0.0001, 203)	93.22 (0.001, 3)	93.75 (0.001, 0.00001, 0.01, 4)	81.25 (0.001, 1, 0.00001, 3)
Giant panda vs Raccoon	80.19 (10000)	52.78 (0.00001, 0.00001, 0.00001)	68.06 (0.0001, 203)	74.31 (0.00001, 163)	68.75 (0.00001, 203)	80.19 (0.001, 3)	64.58 (100000, 0.00001, 0.00001, 2)	89.58 (0.001, 10, 0.0001, 3)
Giant panda vs Rat	83.33 (1)	69.31 (0.00001, 0.00001, 100000)	66.67 (10, 103)	76.39 (0.00001, 123)	68.06 (0.001, 43)	80.5 (0.001, 3)	70.14 (10000, 0.0001, 0.01, 0.25)	84.72 (0.001, 0.1, 0.00001, 43)
Giant panda vs Seal	85.89 (0.1)	56.94 (0.00001, 0.00001, 0.00001)	69.31 (0.0001, 203)	80.56 (0.00001, 183)	77.08 (0.001, 3)	80.19 (0.0001, 3)	80.56 (100000, 0.001, 0.01, 2)	89.58 (1, 1000, 0.0001, 3)
Leopard vs Persian cat	82.19 (0.00001)	79.31 (0.00001, 0.00001, 0.00001)	70.83 (100, 63)	84.72 (0.00001, 203)	77.78 (0.001, 23)	88.19 (0.001, 3)	80.56 (0.00001, 0.00001, 100, 4)	90.97 (0.001, 1, 0.001, 3)
Leopard vs Pig	75 (0.01)	61.39 (0.00001, 0.00001, 0.00001)	61.11 (0.0001, 183)	75 (0.00001, 183)	66.67 (0.001, 3)	72.17 (0.001, 3)	68.75 (0.01, 0.001, 100, 4)	78.47 (0.001, 1, 0.0001, 3)
Leopard vs Hippopotamus	78.17 (10)	50.69 (0.00001, 0.00001, 0.00001)	73.61 (0.0001, 143)	77.08 (0.00001, 143)	74.31 (0.0001, 43)	75.94 (0.0001, 3)	75 (10000, 0.0001, 0.001, 4)	80.56 (0.01, 10, 0.001, 23)
Leopard vs Humpback whale	90.75 (0.00001)	79.31 (0.00001, 0.00001, 0.00001)	89.58 (0.0001, 103)	91.67 (0.00001, 183)	90.97 (0.0001, 143)	90.83 (0.001, 23)	89.58 (100, 0.00001, 0.01, 4)	95.83 (0.001, 10, 0.0001, 3)
Leopard vs Raccoon	80.56 (0.0001)	55 (0.00001, 0.00001, 0.00001)	59.03 (0.0001, 183)	59.03 (0.00001, 143)	69.25 (0.001, 23)	69.25 (0.001, 3)	56.94 (0.01, 0.00001, 0.00001, 0.25)	79.17 (100, 100000, 0.00001, 23)
Leopard vs Rat	76.42 (0.0001)	68.61 (0.00001, 0.00001, 0.00001)	72.22 (10000, 43)	76.39 (0.00001, 183)	68.06 (0.001, 3)	79.86 (0.001, 3)	65.28 (10000, 0.0001, 0.00001, 0.25)	83.33 (0.001, 1, 0.0001, 3)
Leopard vs Seal	80.42 (10000)	63.47 (0.00001, 0.00001, 0.00001)	75.69 (0.0001, 123)	79.86 (0.00001, 143)	75 (0.001, 43)	83.33 (0.001, 3)	81.25 (10000, 0.0001, 0.00001, 0.25)	84.72 (0.001, 1, 0.0001, 3)
Persian cat vs Pig	70 (0.001)	69.31 (0.00001, 0.00001, 0.00001)	63.89 (0.0001, 183)	67.36 (0.00001, 163)	70.14 (0.001, 3)	74.31 (1000, 3)	69.44 (100, 0.00001, 0.01, 4)	73.61 (0.01, 1, 0.00001, 3)
Persian cat vs Hippopotamus	76.81 (0.01)	76.53 (0.00001, 0.00001, 0.00001)	75.69 (1, 63)	79.86 (0.00001, 203)	77.08 (0.01, 3)	78.94 (1, 3)	75.69 (100000, 0.001, 0.00001, 0.25)	80.56 (0.01, 10, 0.001, 23)
Persian cat vs Humpback whale	71.67 (0.00001)	71.39 (0.00001, 0.00001, 0.00001)	81.25 (0.00001, 143)	88.19 (0.00001, 203)	81.94 (0.00001, 143)	81.75 (1, 23)	85.42 (0.01, 0.00001, 0.1, 4)	95.14 (0.001, 1, 0.0001, 3)
Persian cat vs Raccoon	82.64 (0.00001)	79.31 (0.00001, 0.00001, 0.00001)	73.61 (100, 23)	81.25 (0.00001, 163)	69.44 (0.00001, 203)	71.64 (0.001, 3)	65.97 (100000, 0.00001, 0.001, 2)	84.72 (0.001, 0.1, 0.00001, 43)
Persian cat vs Rat	60.44 (0.001)	64.17 (0.00001, 0.00001, 0.00001)	54.86 (0.001, 183)	56.25 (100000, 103)	59.72 (0.001, 3)	60.67 (0.001, 3)	56.94 (100, 0.00001, 10, 0.5)	65.97 (0.0001, 1, 0.0001, 3)
Persian cat vs Seal	80.42 (1)	73.47 (0.00001, 0.00001, 0.00001)	72.22 (0.0001, 183)	71.53 (0.00001, 83)	65.97 (0.01, 63)	72.94 (0.001, 3)	83.33 (10000, 0.00001, 0.01, 4)	84.72 (0.0001, 10, 0.00001, 3)
Pig vs Hippopotamus	71.53 (0.0001)	65.83 (0.00001, 0.00001, 0.00001)	70.14 (0.0001, 83)	65.97 (0.00001, 203)	64.58 (0.0001, 123)	67.36 (0.01, 63)	72.22 (1000, 0.00001, 0.01, 0.25)	83.33 (10, 10000, 0.00001, 3)
Pig vs Humpback whale	80.19 (0.01)	77.92 (0.00001, 0.00001, 0.00001)	82.64 (0.00001, 203)	89.58 (0.00001, 203)	82.64 (0.00001, 203)	80.19 (0.001, 3)	88.89 (100000, 0.001, 0.00001, 0.25)	82.64 (0.1, 1000, 0.0001, 43)
Pig vs Raccoon	71.69 (0.00001)	69.31 (0.00001, 0.00001, 0.00001)	61.11 (0.0001, 43)	72.92 (0.00001, 183)	64.58 (0.0001, 43)	72.22 (10000, 3)	62.5 (0.0001, 0.00001, 0.0001, 4)	81.25 (0.001, 1, 0.00001, 3)
Pig vs Rat	71.53 (0.01)	68.61 (0.00001, 0.00001, 0.00001)	62.5 (1000, 63)	59.72 (0.0001, 203)	57.64 (0.001, 43)	68.06 (0.001, 3)	64.58 (1000, 0.00001, 0.01, 0.25)	63.89 (100, 10000, 0.001, 43)
Pig vs Seal	72.69 (0.01)	65.56 (0.00001, 0.00001, 0.00001)	70.14 (0.00001, 163)	68.06 (0.00001, 183)	72.92 (0.001, 3)	74.31 (0.0001, 3)	72.92 (0.001, 0.001, 0.00001, 4)	78.47 (0.001, 1, 0.00001, 3)
Hippopotamus vs Humpback whale	82.03 (0.01)	80.31 (0.00001, 0.00001, 0.00001)	77.78 (0.0001, 143)	79.86 (0.00001, 143)	81.25 (0.01, 3)	82.81 (0.001, 23)	79.86 (0.001, 0.0001, 10000, 0.25)	88.19 (0.001, 1, 0.00001, 3)
Hippopotamus vs Raccoon	78.47 (0.01)	75.14 (0.00001, 0.00001, 0.00001)	72.22 (0.0001, 203)	70.14 (0.00001, 183)	78.47 (0.001, 3)	80.94 (0.001, 23)	75.69 (0.00001, 0.001, 1, 4)	77.78 (0.01, 1000, 0.001, 43)
Hippopotamus vs Rat	75.33 (100)	75.83 (0.00001, 0.00001, 0.00001)	65.28 (1000, 43)	71.53 (0.00001, 183)	70.14 (0.01, 23)	70.25 (0.001, 3)	64.58 (100000, 0.00001, 0.1, 4)	81.25 (0.001, 0.1, 0.0001, 3)
Hippopotamus vs Seal	69.44 (0.01)	49.31 (0.00001, 0.00001, 0.00001)	58.33 (0.1, 63)	65.28 (0.00001, 183)	61.81 (0.001, 43)	70.83 (0.001, 3)	60.42 (0.001, 0.01, 0.00001, 4)	61.81 (0.001, 1, 0.00001, 63)
Humpback whale vs Raccoon	85.67 (0.00001)	80.69 (0.00001, 0.00001, 10000)	84.03 (0.00001, 83)	90.97 (0.0001, 123)	90.97 (0.0001, 83)	81.94 (0.001, 3)	83.33 (10000, 0.0001, 0.01, 0.25)	93.06 (10, 100000, 0.00001, 3)
Humpback whale vs Rat	82.28 (0.01)	80.31 (0.00001, 0.00001, 0.00001)	81.94 (0.0001, 183)	86.11 (0.00001, 203)	81.94 (0.0001, 183)	80.58 (100, 3)	77.78 (100000, 0.001, 10, 0.25)	90.97 (0.001, 0.01, 0.0001, 3)
Humpback whale vs Seal	76.39 (0.01)	72.08 (0.00001, 0.00001, 0.00001)	77.78 (0.0001, 143)	73.61 (0.00001, 203)	78.47 (0.0001, 143)	79.17 (0.0001, 3)	78.47 (100000, 0.0001, 0.001, 0.25)	80.56 (0.01, 100, 0.0001, 3)
Raccoon vs Rat	62.22 (100)	61.89 (0.00001, 0.00001, 0.00001)	59.72 (100, 43)	70.83 (0.00001, 163)	61.81 (0.001, 163)	60.22 (0.001, 3)	65.28 (100000, 0.00001, 10, 4)	70.83 (0.001, 0.1, 0.0001, 3)
Raccoon vs Seal	90.28 (100)	75.39 (0.00001, 0.00001, 100000)	78.47 (0.00001, 183)	84.03 (0.00001, 183)	82.64 (0.001, 63)	80.28 (0.001, 3)	75.69 (100000, 0.00001, 0.01, 4)	88.19 (100, 100000, 10, 43)
Rat vs Seal	70.86 (0.001)	65.17 (0.00001, 0.00001, 0.00001)	68.75 (0.00001, 183)	68.75 (0.00001, 143)	68.75 (0.01, 3)	67.83 (0.01, 3)	69.87 (100000, 0.001, 0.01, 0.25)	81.25 (0.0001, 0.1, 0.00001, 3)
Average ACC	77.46	64.31	71.74	75.99	72.87	77.46	73.33	83.29
Average Rank	3.46	6.84	5.99	4.32	5.22	3.59	5.02	1.56

[†] represents the proposed model.